Title

Tropical cyclogenesis in warm climates simulated by a cloud-system resolving model

Journal

Climate Dynamics, 52(1-2)

ISSN

0930-7575

Authors

Fedorov, Alexey V
Muir, Les
Boos, William R
et al.

Publication Date

2019

DOI

10.1007/s00382-018-4134-2

Peer reviewed

Tropical cyclogenesis in warm climates simulated by a cloud-system resolving model

Alexey V. Fedorov[1] · Les Muir[1] · William R. Boos[2] · Joshua Studholme[1,3]

1 Department of Geology and Geophysics, Yale University, 210 Whitney Ave, New Haven, CT 06511, USA

2 Department of Earth & Planetary Science, University of California Berkeley, 307 McCone Hall, Berkeley, CA 94720, USA

3 Department of Physics, Shirshov Institute of Oceanology, Russian Academy of Sciences, 36 Nakhimovsky Ave, Moscow 117997, Russian Federation

Abstract

Here we investigate tropical cyclogenesis in warm climates, focusing on the effect of reduced equator-to-pole temperature gradient relevant to past equable climates and, potentially, to future climate change. Using a cloud-system resolving model that explicitly represents moist convection, we conduct idealized experiments on a zonally periodic equatorial β-plane stretching from nearly pole-to-pole and covering roughly one-fifth of Earth's circumference. To improve the representation of tropical cyclogenesis and mean climate at a horizontal resolution that would otherwise be too coarse for a cloud-system resolving model (15 km), we use the hypohydrostatic rescaling of the equations of motion, also called reduced acceleration in the vertical. The simulations simultaneously represent the Hadley circulation and the intertropical convergence zone, baroclinic waves in mid-latitudes, and a realistic distribution of tropical cyclones (TCs), all without use of a convective parameterization. Using this model, we study the dependence of TCs on the meridional sea surface temperature gradient. When this gradient is significantly reduced, we find a substantial increase in the number of TCs, including a several-fold increase in the strongest storms of Saffir–Simpson categories 4 and 5. This increase occurs as the mid-latitudes become a new active region of TC formation and growth. When the climate warms we also see convergence between the physical properties and genesis locations of tropical and warm-core extra-tropical cyclones. While end-members of these types of storms remain very distinct, a large distribution of cyclones forming in the subtropics and mid-latitudes share properties of the two.

Keywords

Tropical cyclones, Climate change, Atmospheric modeling, Paleoclimate

1 Introduction

Understanding tropical cyclogenesis in a climate warmer than that of the present represents a challenging problem both from theoretical and numerical modeling perspectives. The difficulties are several-fold. First, we need to understand how the atmospheric general circulation changes with future or past climate change—an issue complicated by biases common in

simulations of global climate models (GCMs; e.g. Burls et al. 2016). Second, computing power is currently insufficient to provide the spatial resolutions needed to successfully simulate moist convective motions in GCMs, leading to the nearly universal use of convective parameterizations in global models with just a few exceptions (e.g. Miyamoto et al. 2014), which affects how these models simulate both the atmospheric mean state and tropical cyclones (e.g. Kim et al. 2012). To provide one way of circumventing these issues, here we employ a cloud-system resolving model integrated in a large, idealized domain and focus on just one aspect of the problem—the dependence of tropical cyclones (TCs) on the meridional gradient in sea surface temperature (SST).

Given the vast impacts of TCs, the question of future changes in the global distribution, strength, and frequency of these storms is actively debated. Yet, insufficient model resolution is a big obstacle to addressing this question since explicit representation of the TC eyewall, with its O(10 km) size, is at present too computationally expensive for global GCMs. Consequently, even the latest generation of those models typically only simulate TC-like storms (e.g. Walsh et al. 2007, 2013; Gualdi et al. 2008; Scoccimarro et al. 2011; Camargo et al. 2013; Shaevitz et al. 2014; Huang et al. 2017). Although the spatial and temporal distribution of these storms generally resembles the distribution of observed TCs, frequently there are biases in those distributions and the model storms are typically larger in size and weaker than observed (e.g. Walsh et al. 2015). In fact, whether a GCM can simulate strong TCs often depends on the tuning of the convective parameterization or numerical scheme (Kim et al. 2012).

Regional atmospheric models can be run at higher resolutions, on the order of 20 km, but with no convective parameterization they still typically fail to reproduce strong cyclones. For example, in several regional models integrated at the relatively fine horizontal resolution of 18 km, the most intense storms corresponded to Saffir–Simpson category 3 (Knutson et al. 2007; Wu et al. 2014). Thus, the question of how the characteristics of the most intense TCs (i.e. categories 4 and 5) vary with the global climate state cannot be answered directly by global and most regional numerical models.

Downscaling methodologies have been used in attempts to circumvent this problem, using grid-scale fields from coarse-resolution global models as inputs to statistical or dynamical simulations of individual TCs (e.g. Emanuel et al. 2008; Fedorov et al. 2010; Bender et al. 2010; Zhao et al. 2010; Villarini and Vecchi 2012; Knutson et al. 2013). Additionally, various indirect metrics for assessing TC activity, from maximum Potential Intensity (PI, e.g. Emanuel 1988, 1995; Bister and Emanuel 1998) to Genesis Potential Indices (GPI, Emanuel and Nolan 2004; Tippett et al. 2011), have been broadly used to examine the effects of both present and past climate change (e.g. Knutson and Tuleya 2004; Emanuel 2005; Bengtsson et al. 2007; Vecchi and Soden 2007; Korty et al. 2008).

Overall, many studies using different methodologies suggest that there will be a reduction in the frequency of TCs and a possible, but not certain increase in peak TC intensity during the twenty-first century in response to contemporary global warming (e.g. Sugi et al. 2002; Yoshimura and Sugi 2005; Bengtsson et al. 2007; Held and Zhao 2011; Murakami et al. 2014; Camargo 2013; Tory et al. 2013). Some studies however indicate an increase in TC frequency (e.g. Emanuel 2013a, b). The problem is complicated by the strong sensitivity of TC activity to the horizontal and vertical structure of the patterns of warming and changes in vertical wind shear (e.g. Vecchi and Soden 2007; Sugi et al. 2009; Camargo et al. 2014a, b).

A number of studies examined tropical cyclogenesis in the idealized setting of an aqua-planet. For example, Merlis et al. (2013) studied the effect of climate change on tropical cyclogenesis on an aqua-planet using a slab-ocean atmospheric GCM (with convective parameterization) at 50 km horizontal resolution and with a time-invariant distribution of prescribed ocean heat flux convergence (i.e. a fixed q-flux). In such a model configuration the Intertropical Convergence Zone (ITCZ) moves northward when the radiative forcing (solar constant or CO_2 concentration) is increased, leading to a monotonic increase in TC activity. The same model was used by Ballinger et al. (2015) to examine the sensitivity of TC activity to off-equatorial SST anomalies.

In parallel, a number of studies investigated TC activity on a spherical aqua-planet with uniform SSTs (e.g. Shi and Bretherton 2014; Arnold and Randall 2015; Merlis et al. 2016 GRL). In particular, Merlis et al. (2016) find that the region of peak TC genesis is in the tropics off the equator, but shifts poleward and (perhaps surprisingly) decreases in magnitude as the uniform SST increases. The TCs also drift poleward and accumulate in the polar regions, so that the peak TC number is actually highest near and poleward of 60° latitude.

Other studies attempted to explore tropical cyclogenesis in past warm climates. For example, Korty et al. (2008) conducted sensitivity studies using a coarse-resolution GCM with modern boundary conditions but high CO_2 forcing, typical of the Eocene epoch, wherein they parameterized the effect of TCs on upper-ocean vertical mixing. Although they did not simulate TCs directly, their results showed a significant increase and poleward expansion of maximum potential intensity.

Kiehl et al. (2012) looked at extreme weather phenomena, including hurricanes, within coupled climate model simulations of the Paleocene-Eocene Thermal Maximum (PETM) using Community Atmospheric Model (CAM4) simulations at 0.5° horizontal resolution. The model simulated warm tropical SSTs approaching 40 °C. They concluded that the warm, moist tropical environment of the PETM created conditions favorable for tropical cyclogenesis.

Fedorov et al. (2010) used a combination of atmospheric GCM experiments with a downscaling approach to study tropical cyclogenesis during the early Pliocene epoch, when there was a strong reduction of the meridional SST gradient (Brierley et al. 2009; Fedorov et al. 2015) under atmospheric CO_2 levels within the range 350–450 ppm. They found a doubling of the total number of TCs and a significant increase in strong cyclones. A more recent study of Yan et al. (2016) used a TC-permitting atmospheric GCM to confirm enhanced TC activity during the Pliocene.

While these studies represent gradual progress in our understanding of tropical cyclogenesis, large uncertainty persists. Uncertainty in the proxy observations and boundary conditions of the past, and diversity in the response of climate model simulations to a given forcing make it difficult to assess robust patterns of change in the hydrological cycle, including changes in the ITCZ structure and intensity (e.g. Carmichael et al. 2016; Burls and Fedorov 2017). Computational limitations, the relatively coarse resolution of GCMs, and uncertainties due to parameterizations of sub-grid scale processes further complicate the projection of TC changes.

As mentioned already, here we confine our approach to aqua-planet simulations using a cloud-system resolving model without convective parameterization. To reduce computational costs we use an idealized, zonally periodic, equatorial β-plane that covers just one-fifth of Earth's circumference in the zonal direction—large enough to represent one or two typical mid-latitude baroclinic waves.

The model is run at a horizontal resolution of 15 km, which could be categorized as being in the "gray zone" between the O(1 km) resolutions needed for cloud-system resolving models and the O(100 km) resolutions at which moist convection is parameterized (Sun et al. 2013). Previous studies have shown (Gentry and Lackmann 2010; Fierro et al. 2009; Boos et al. 2016) that in order to reproduce TCs realistically, a model without convective parameterization needs to have a horizontal resolution on the order of 1 km —a resolution computationally prohibitive for simulations on a global scale. To address this problem we use the Reduced Acceleration in the Vertical (RAVE) approach, which scales the left-hand side of the vertical momentum equation by a factor $\gamma > 1$ ("Appendix 1"). Because RAVE artificially increases the inertia of air parcels it is also referred to as the hypohydrostatic rescaling, with $\gamma = 0$ corresponding to hydrostatic balance. In effect, RAVE reduces the scale separation between large-scale and convective-scale motions, allowing explicit representation of both in the same model (e.g. Kuang et al. 2005; Pauluis and Garner 2006; Garner et al. 2007).

Recently, in simulations with doubly periodic domains, Boos et al. (2016) showed that RAVE makes possible simulations of the most intense TCs (i.e. category 5) in a cloud-system resolving model without convective parameterization at O(10 km) resolution. Here, we build on their results and use RAVE to study tropical cyclogenesis on a global scale.

The structure of this paper is as follows. The next section presents details of the numerical model and its configuration. The subsequent section shows results from our simulations forced by different meridional SST gradients. We then describe the simulated changes in tropical cyclogenesis as well as the relationship between tropical and extra-tropical cyclones. The paper ends with a discussion of the implications of our study for contemporary and past climate change.

2 Model details

This study uses the System for Atmospheric Modeling (SAM) v6.3 (Khairoutdinov and Randall 2003), which integrates the anelastic equations of motion in Cartesian coordinates. Previous studies have used this model to simulate radiative–convective equilibrium and explore convective self-aggregation and spontaneous cyclogenesis, for example (Bretherton et al. 2005; Muller and Held 2012; Boos et al. 2016). A nearly global configuration of this model with a 4 km resolution was recently used to study realistically organized tropical convection for latitudinally varying SSTs within relatively short 30-day integrations (Bretherton and Khairoutdinov 2015).

The model has prognostic equations for liquid/ice water moist static energy, total precipitating water, and non-precipitating water. A five-class bulk microphysics scheme diagnoses cloud water and ice, rain, snow, and graupel. Fully interactive radiation is based on parameterizations from the National Center for Atmospheric Research (NCAR) Community Climate Model (CCM) version 3.5 (Kiehl et al. 1998) with radiative fluxes calculated at least once every 5 min (the radiation code is called every five time steps). Ocean surface albedo depends on solar zenith angle. Although use of interactive radiation does not alter SST, moisture-dependent radiation has been shown to be essential for achieving self-aggregation of convection in SAM (Bretherton et al. 2005; Wing and Emanuel 2014; Emanuel et al. 2014).

We should note that the model representations of damping, radiative transfer and other model characteristics might potentially affect some of our results, as other studies have shown that these sensitivities are not always straightforward (Zhao et al. 2012).

The model horizontal resolution is 15 km and the time step ranges from 4 to 50 s, depending on numerical stability, with SAM automatically halving the time step when high Courant numbers are achieved. The integrations have 64 vertical levels, with vertical grid spacing ranging from 80 m near the surface to 400 m in the bulk of the troposphere and 1.2 km near the rigid lid at 27 km. To reduce gravity wave reflection and resonance, Newtonian damping is applied to winds, temperature, and water vapor in the top 30% of the domain (in height) with a time scale that decays linearly from 2 min at the top to 2 h at the bottom of this sponge layer. A Smagorinsky-type closure is used to represent subgrid-scale turbulence, with the parameterized stresses scaled by the RAVE factor γ to account for the fact that RAVE alters

the aspect ratio of the resolved eddies (see discussion in appendix of Pauluis and Garner 2006).

This model was recently used to study the effect of RAVE rescaling and model horizontal resolution on convective self-aggregation and tropical cyclogenesis in relatively small, doubly periodic square domains (Boos et al. 2016). These authors argued that the rescaling improves simulations of TCs by moistening the troposphere, which eliminates a dry bias that otherwise develops in cloud-system resolving simulations with a relatively coarse model resolution (e.g. at grid spacings of 5–20 km). Here we use SAM with the RAVE rescaling in a large aqua-planet domain. For the results described in the main body of this study, we use the RAVE factor $\gamma = 15$, which for a horizontal grid spacing of 15 km could be argued to rescale the equations of motion to yield an "equivalent" horizontal grid spacing of 1 km (e.g. Pauluis and Garner 2006). Furthermore, $\gamma = 15$ produces a mean climate state most closely mimicking the observed tropical state during boreal summer, with one ITCZ that is located north of the equator. In the "Appendix 1" we show how some of these results change when we go from $\gamma = 1$ (no rescaling) to $\gamma = 5$ and 15. In addition, we investigated the sensitivity of the model to using a higher horizontal resolution of 10 km within a small number of shorter simulations but did not find any significant differences.

The model domain is a zonally periodic β-plane with rigid walls at the northern and southern boundaries at roughly 70°N and 70°S (Figs. 1, 2). Its zonal width is 8000 km. Each simulation lasts 1800 days (60 months). There is no seasonal cycle in the model—the simulations are set to describe a perpetual July (or more accurately, an average of June, July, August). Thus, each simulation reproduces an equivalent of about 20 boreal summers. Since we use zonally-uniform, fixed SSTs (see next), interannual and decadal variations in the number and strength of simulated TCs are relatively minor. Consequently, the length of integration (20 seasons) is sufficiently long to produce robust statistics.

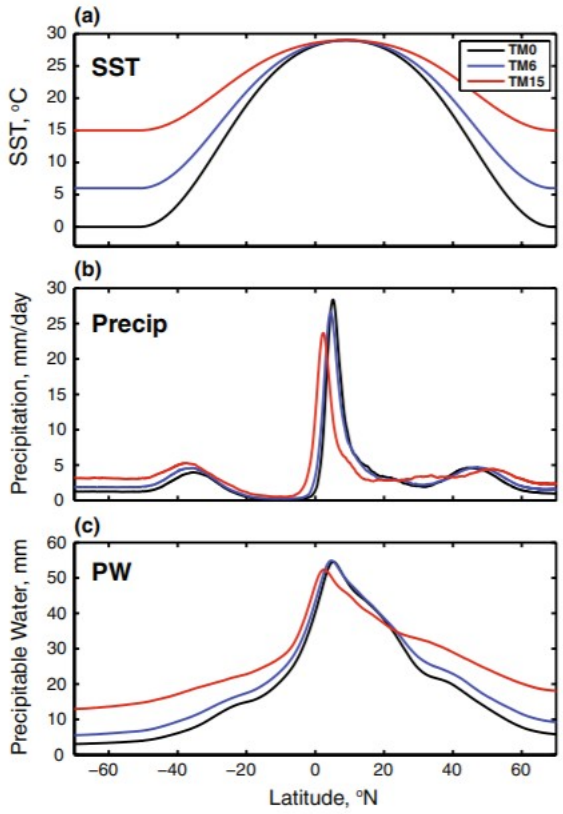

Fig. 1 Meridional distribution of **a** the prescribed sea surface temperature (°C), and the simulated zonal means of **b** precipitation (mm/day) and **c** precipitable water (mm) for the three simulations with T_{min} = 0 °C (black), T_{min} = 6 °C (blue), and T_{min} = 15 °C (red). Hereafter, these simulations are referred to as TM0, TM6, and TM15. TM0 describes a climate state corresponding to a modern perpetual July. Each simulation lasts 20 boreal summers. Note that the ITCZ in these simulations moves closer to the equator for warmer climates, which is consistent with a greater humidity increase on the southern flank of the ITCZ

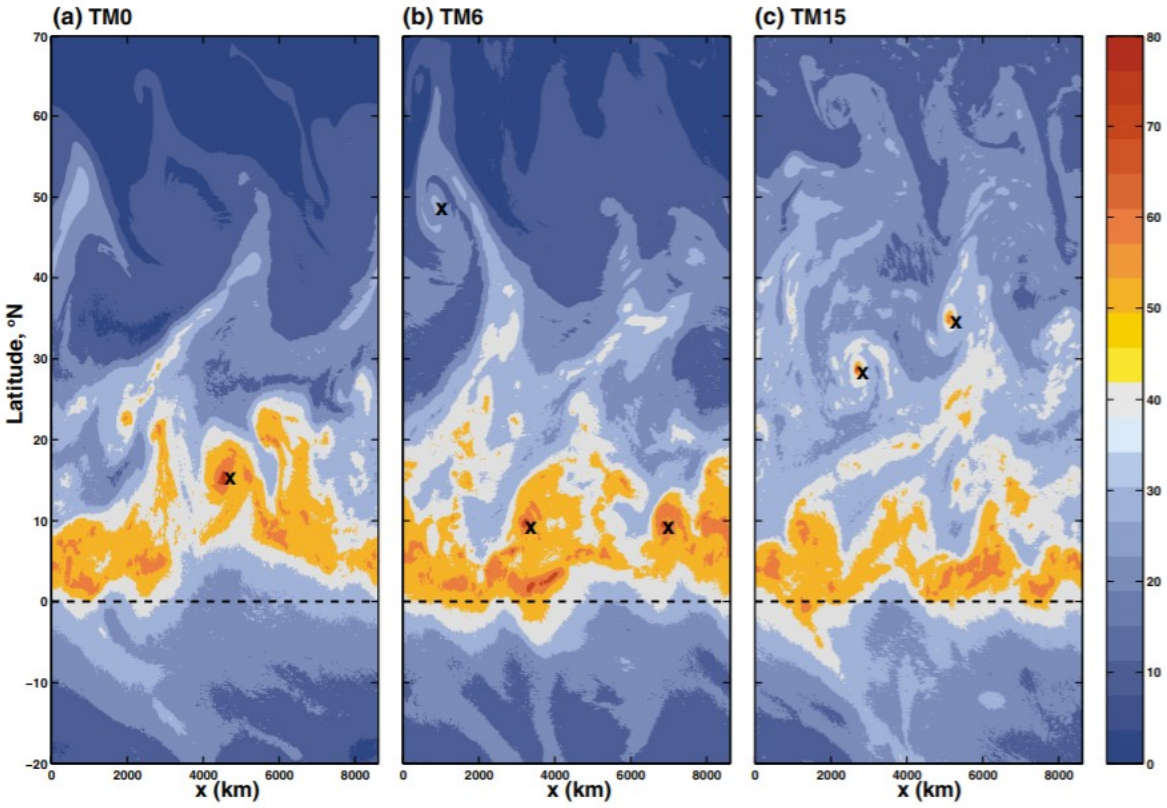

Fig. 2 Snapshots of precipitable water (in mm) simulated by the model on day 208 in simulations **a** TM0, **b** TM6, and **c** TM15. Black crosses mark several tropical and extra-tropical warm-core cyclones. The ITCZ stays north of the equator. Also note typical baroclinic waves in mid-latitudes. The full model domain extends from 70°S to 70°N

For oceanic lower boundary conditions we apply wind-dependent surface sensible and latent heat fluxes computed using a bulk surface flux formula with a fixed minimum surface wind speed of 1 m/s. Different idealized profiles of SST as a function of latitude are prescribed, following an approach originally proposed by Neale and Hoskins (2000):

$$SST = T_{min} + (T_{max} - T_{min}) \left(1 - 0.5 \sin^2 \left(\frac{3}{2}(\varphi - \varphi_{max})\right) - 0.5 \sin^4 \left(\frac{3}{2}(\varphi - \varphi_{max})\right)\right)$$

$$\text{and } SST = T_{min} \text{ for } |\varphi - \varphi_{max}| \geqslant 60^o.$$

where φ is latitude, $\varphi_{max} = 9^o$ and T_{max} = 29 °C.

This expression describes profiles close to Gaussian with the maximum temperature T_{max} shifted off the equator by φ_{max} to the north and tapered to a constant temperature T_{min} in high latitudes (Fig. 1a). Since we focus on the effect of reductions in the meridional SST gradient, we do not change the maximum SST in low latitudes, which stays at 29 °C. For T_{min} = 0 °C this expression yields a profile that approximates modern zonal-mean conditions

averaged for June, July, and August (later on it is referred to as “perpetual July”).

3 Results: simulation of different mean climates

We conduct three idealized simulations that differ in the strength of the meridional SST gradient—a modern climate with high-latitude temperature T_{min} = 0 °C, a warmer climate with T_{min} = 6 °C, and a very warm climate with T_{min} = 15 °C (T_{min} gives the coldest SST of the simulation). We refer to these simulations as TM0, TM6 and TM15, respectively (Fig. 1). The meridional SST gradient in TM0 was constructed to roughly match that of the observed zonal mean SST in the modern climate (Neale and Hoskins 2000); since the maximum SST is displaced into the northern hemisphere, we consider TM0 an idealized analogue of the modern boreal summer (perpetual July) SST distribution in the Pacific.

For the TM0 SST distribution, the model simulates the mean position of the ITCZ at about 5°N, close to the SST maximum (Fig. 1b). The northern hemisphere also contains more precipitable water overall (Fig. 1c). The ITCZ constantly meanders around its mean position, which leads at times to localized convective aggregation and cyclogenesis (Fig. 2). There are also strong baroclinic waves in mid-latitudes, associated with pronounced synoptic storms that contribute to the secondary maximum in zonal mean precipitation near 45°N (Fig. 1b).

As expected, the Hadley circulation is dominated by the cross-equatorial winter cell extending from the ITCZ to the subtropical southern hemisphere (Fig. 3a), presumably driven by the stronger meridional SST gradient extending across the equator into the southern hemisphere. Similarly, the upper tropospheric mid-latitude westerly jet (Fig. 4a) is also stronger in the southern hemisphere, consistent with thermal wind balance and typical boreal winter conditions.

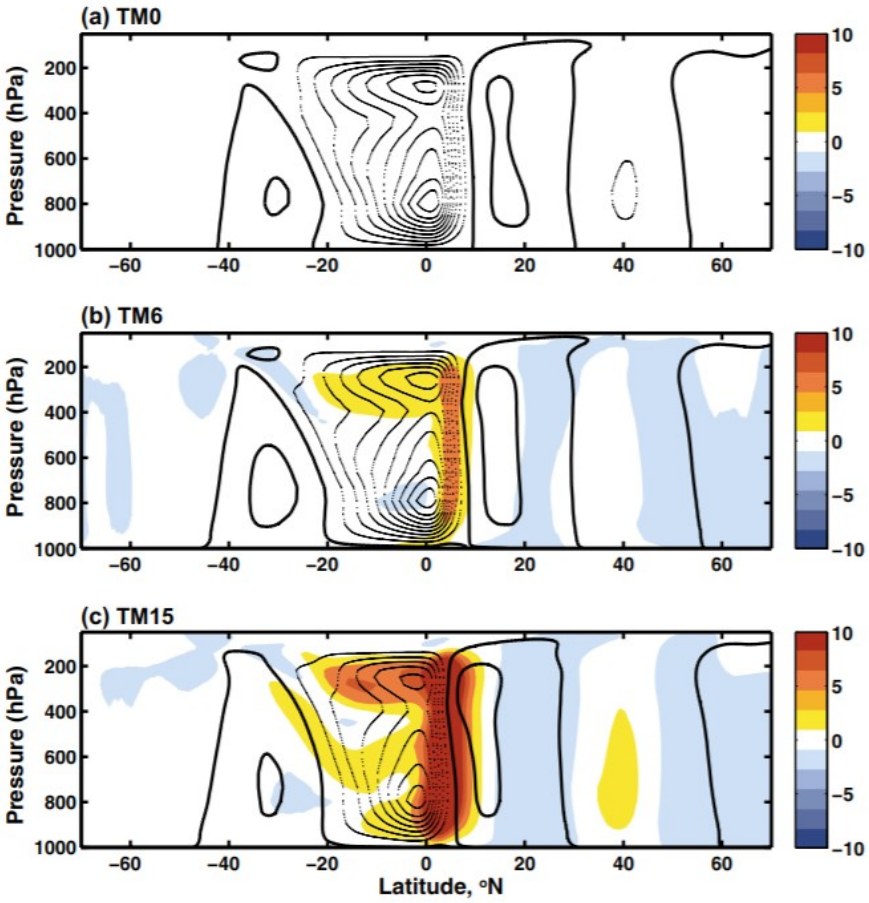

Fig. 3 Zonally-averaged stream function for TM0 (black solid and dashed contours indicating positive and negative values with 5×10^{10} kg s^{-1} contour interval) and corresponding anomalies (colors, units of 10^{10} kg s^{-1}) in **a** TM0, **b** TM6, and **c** TM15. The stream function anomalies imply the southward shift of the Hadley circulation and a weakening of the winter Hadley cell in the warmer climates

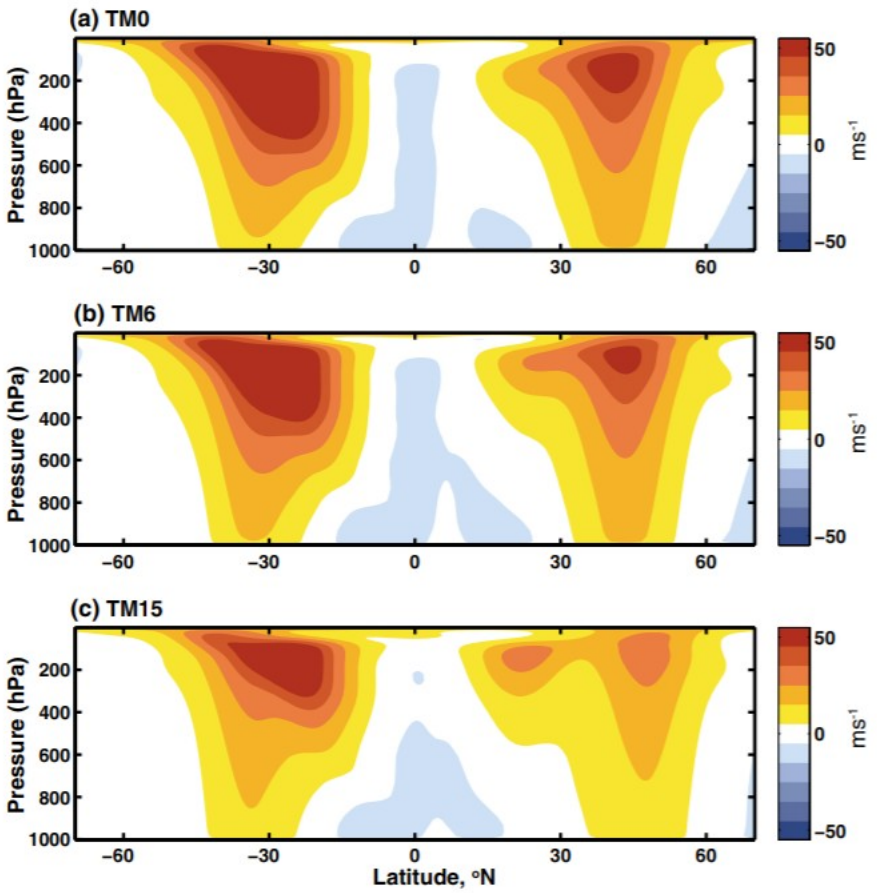

Fig. 4 Zonally-averaged wind speed in simulations **a** TM0, **b** TM6, and **c** TM15. Note the weakening of the jet streams and the split of the northern jet into distinct subtropical and polar jets in the warmer climates

When we increase high-latitude temperature and reduce the meridional SST gradient, several important changes occur. In particular, the Hadley circulation and the zonal jets weaken in response to the weaker temperature gradient (Figs. 3, 4). In addition, the upper tropospheric jet in northern mid-latitudes splits into two weaker jets—subtropical and polar. Such separation is, at best, barely visible in the zonally averaged representation of zonal flow in the simulation forced by the strongest SST gradient (TM0; Fig. 4a).

In the tropics, the ITCZ weakens in response to the reduction in meridional SST gradient, perhaps responding to the broadening of the SST maximum. The ITCZ also shifts a few degrees of latitude southward, still staying north of the equator (Figs. 1, 2). This shift is accompanied by a greater increase in precipitable water on the southern flank of the ITCZ than on the northern flank; precipitable water actually decreases just north of the ITCZ (Fig. 1c). In the next sections we will describe how these and other changes are associated with changes in tropical cyclogenesis.

4 Results: tropical and extra-tropical cyclogenesis

All of our simulations produce a full range of tropical cyclone intensities in the northern hemisphere, up to Saffir–Simpson categories 4 and 5 (Figs. 5, 6; the method used to identify and track cyclones is described in “Appendix 2”).

Well-defined TC eyes and eyewalls are simulated in many of these storms (e.g. Fig. 5b). On some occasions TCs are shed from the ITCZ and then travel northward, on other occasions they are generated well north of the ITCZ. At the same time, a significant number of warm-core storms develop in mid-latitudes, some of which could even be classified as Saffir–Simpson category 1 in terms of their surface wind speed (we will refer to these as warm-core extra-tropical cyclones, ETCs). The ETCs develop in mid-latitudes, in our simulations north of 40°N (Figs. 7, 15 of “Appendix 2”). Their origin is related to baroclinic waves, as seen in an example marked in Fig. 2b (upper left corner), when warm moist air is drawn into the center of a synoptic storm. Such storms are sometimes referred to as warm seclusion extra-tropical cyclones (e.g. Maue and Hart 2005).

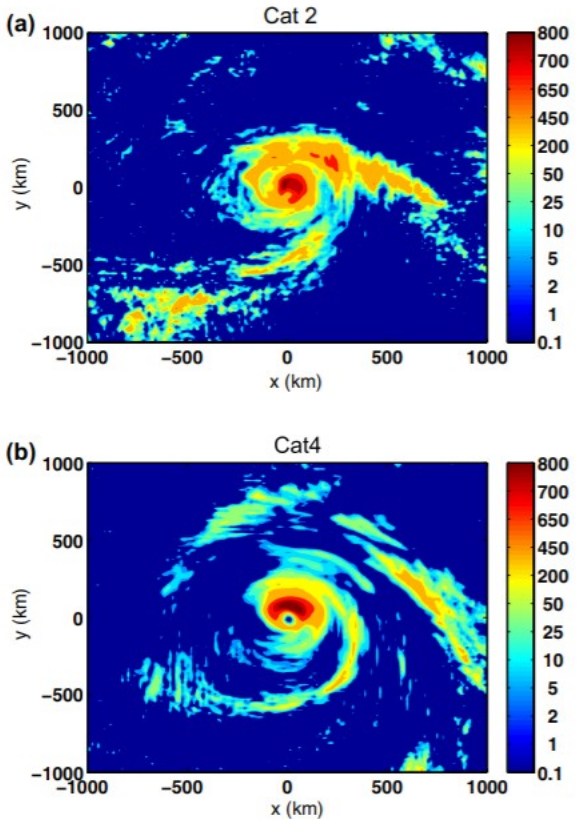

Fig. 5 Examples of the simulated precipitation field (mm/day, a 6-h average) for category 2 and 4 tropical cyclones. A log color scale is used. Well defined precipitation bands and the hurricane eye are clearly visible for the stronger storm

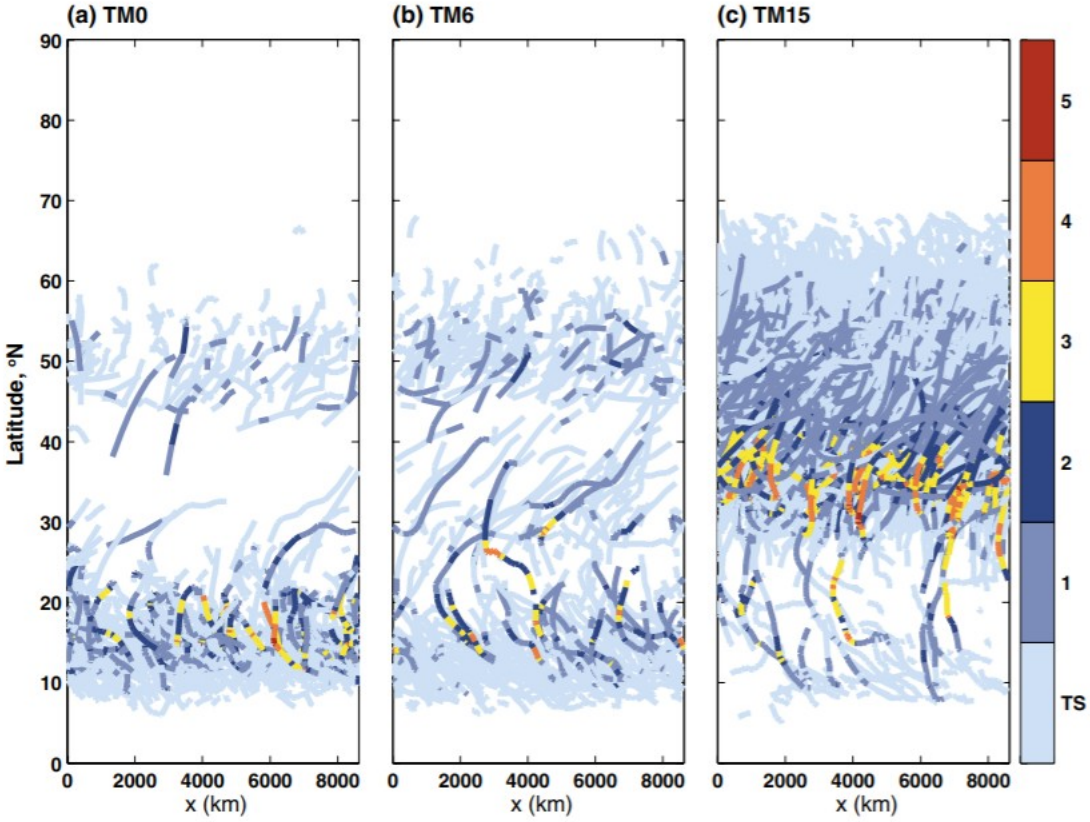

Fig. 6 The tracks of identified warm-core cyclones in the northern hemisphere, colored according to the storm's Saffir–Simpson category for **a** TM0, **b** TM6, and **c** TM15. Each simulation lasts 20 boreal summers and uses perpetual July SSTs as the prescribed forcing. The locations of tracks of tropical and extra-tropical storms (TCs and ETCs) are well separated geographically in the first two simulations, but not in TM15. Also note the new active region of TC formation and growth that emerged in mid-latitudes (the 30-40°N band) in the last simulation

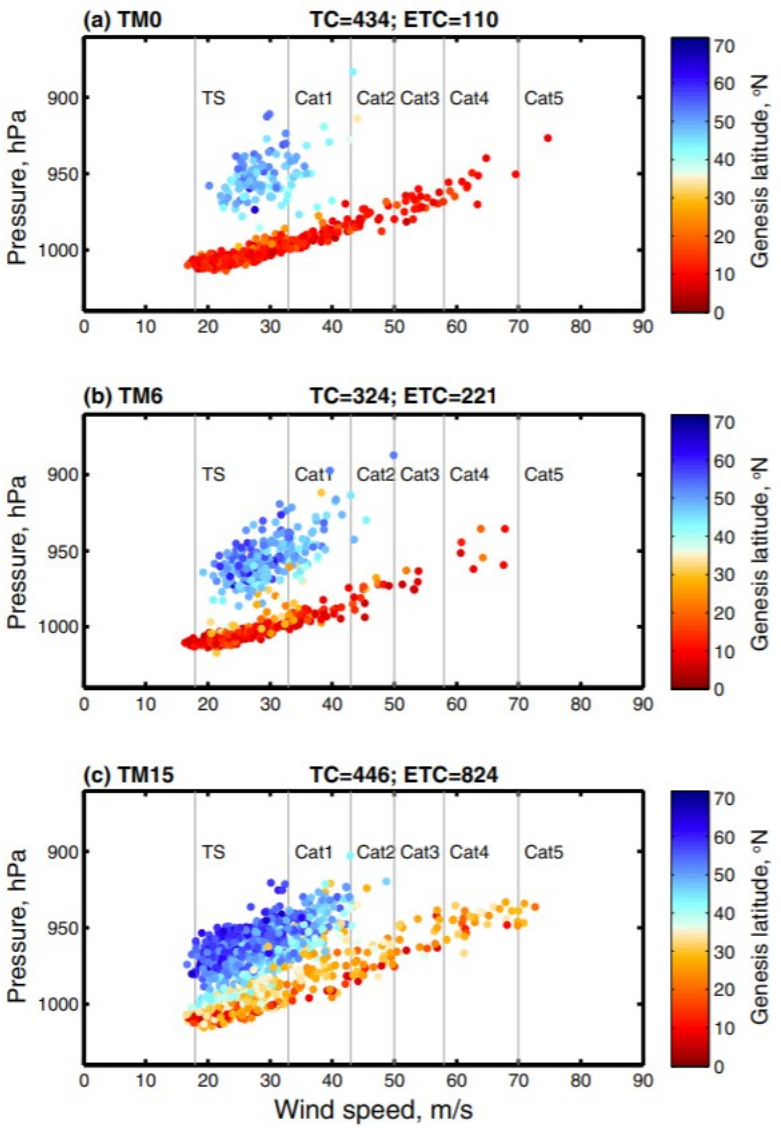

Fig. 7 Scatterplots of maximum surface wind speed (m/s) versus minimum central surface pressure (mb) for the identified warm-core cyclones in simulations **a** TM0, **b** TM6, and **c** TM15. Each cyclone is colored according to its genesis latitude; the Saffir–Simpson categories are also shown. The two distinct distributions corresponding to tropical and warm-core extra-tropical storms converge in TM15. The numbers at the top of each panel refer to the total number of tropical (TC) and extra-tropical (ETC) cyclones in the simulations. Note a significant increase in the frequency of strong storms of categories 4 and 5 in TM15

The tropical and extra-tropical storms fall into two different, very distinct distributions, both in terms of their typical genesis locations and physical properties. The simulated TC distribution for the strongest SST gradient shows the classical tight relationship between minimum central pressure and maximum surface wind speed, with a near linear or weakly quadratic form that closely resembles observations (e.g. Knutson et al. 2007). In contrast, the warm-core ETCs exhibit not as tight a relationship with a different slope and generally weaker wind speed for the same minimum central pressure, which reflects the broader spatial structure of the extra-tropical storms (Fig. 8a, b).

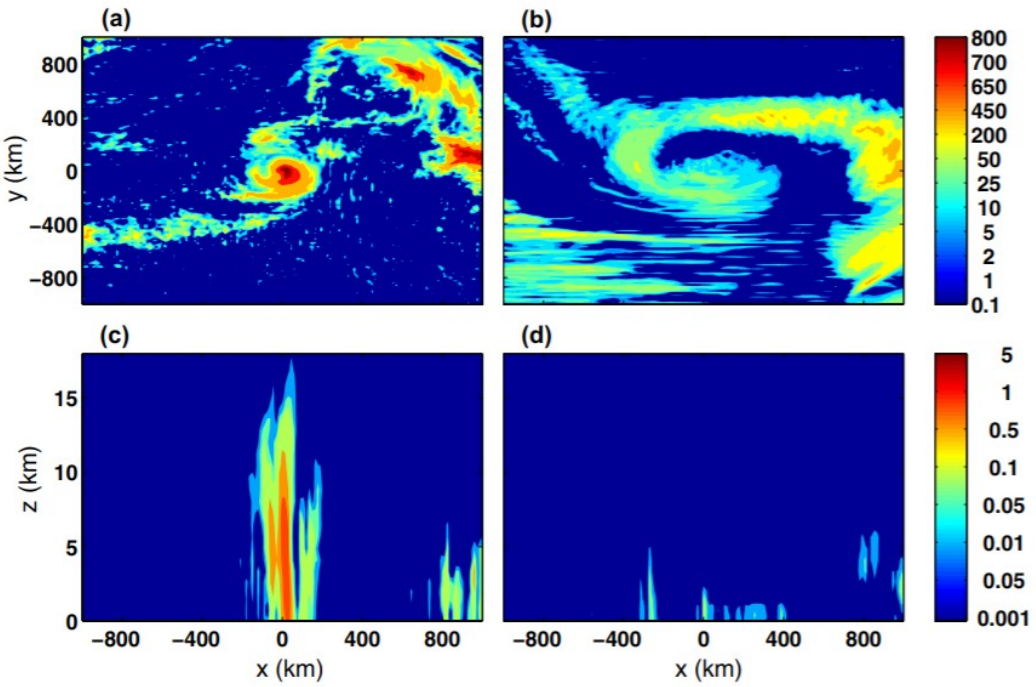

Fig. 8 Examples of Category 1 tropical and extra-tropical warm-core cyclones (left and right, respectively) within the TM0 simulation showing different horizontal and vertical structure of the storms (top and bottom). **a, b** precipitation (mm/day) and **c, d** precipitating water (g/kg) along the latitude passing through the core of the storms (y = 0). Note large differences in both the vertical and spatial structures of the two types of storms

Spatially, the asymmetric frontal structure of the extra-tropical storms contrasts with the more confined, axisymmetric structure of the TCs. Similarly, in the vertical plane, TCs exhibit a deep coherent structure extending up to the tropopause, which contrasts with the typical shallow depth of ETCs (Fig. 8c, d).

A formal cluster analysis of the identified cyclones, based on the relationship between the 200 and 800 hPa geopotential heights, also confirms that these two types of storms belong to two distinct clusters with different physical characteristics, well separated in the modern climate (for details of the cluster analysis see “Appendix 2”). Note that the cluster analysis does not use the TC genesis latitude as a parameter, focusing on the physical characteristics of the storms rather than their locations. Next, we will investigate changes in the simulation of TCs and their relationship to extra-tropical storms as the meridional SST gradient weakens. The cluster analysis will provide the total counts of the two types of storms in the simulations (Table 1).

Table 1 The number of identified warm-core cyclones in different experiments, including tropical (TC) and extra-tropical (ETC)

	TM0	TM6	TM15
TC	434	324	446
ETC	110	221	824
Total	544	545	1270

As we reduce the meridional SST gradient, the distribution of TCs changes in several important ways, albeit not necessarily monotonically. Going from TM0 to TM6 reduces the total number and intensity of TCs (Fig. 9), from 434 to 324. This occurs concurrently with a weakening and a small equatorward shift of the ITCZ (Fig. 1b), and previous studies have argued that an equatorward shift of the ITCZ will cause a reduction in TC genesis frequency (Merlis et al. 2013). The Genesis Potential Index (GPI), here defined as in Emanuel and Nolan (2004), which provides a statistical prediction of TC genesis frequency based on climatological mean variables, decreases in the region of active TC genesis between 5° and 15°N, largely because of changes in relative humidity (Fig. 10d, e). (Note that since GPI is based on an empirical fit to modern data, hereafter it is only used as a qualitative indicator.)

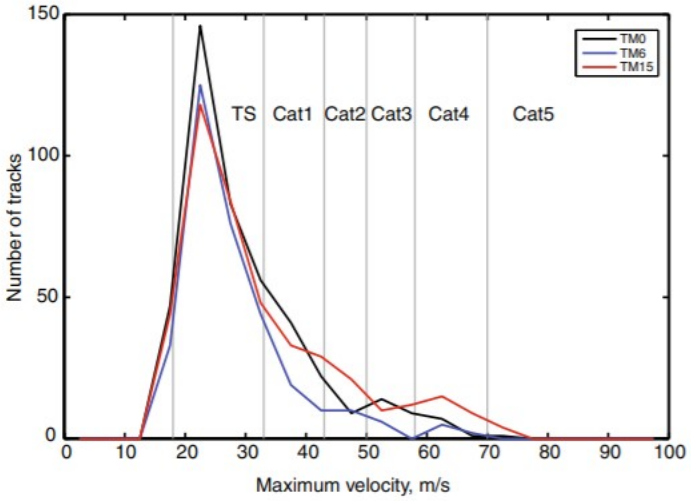

Fig. 9 The distribution of tropical cyclones according to their maximum strength for simulations TM0 (black), TM6 (blue), and TM15 (red). The total TC numbers in these simulations are 434, 323 and 446, respectively. The graph highlights a significant increase in the number of strong tropical cyclones, categories 2 through 5, in TM15

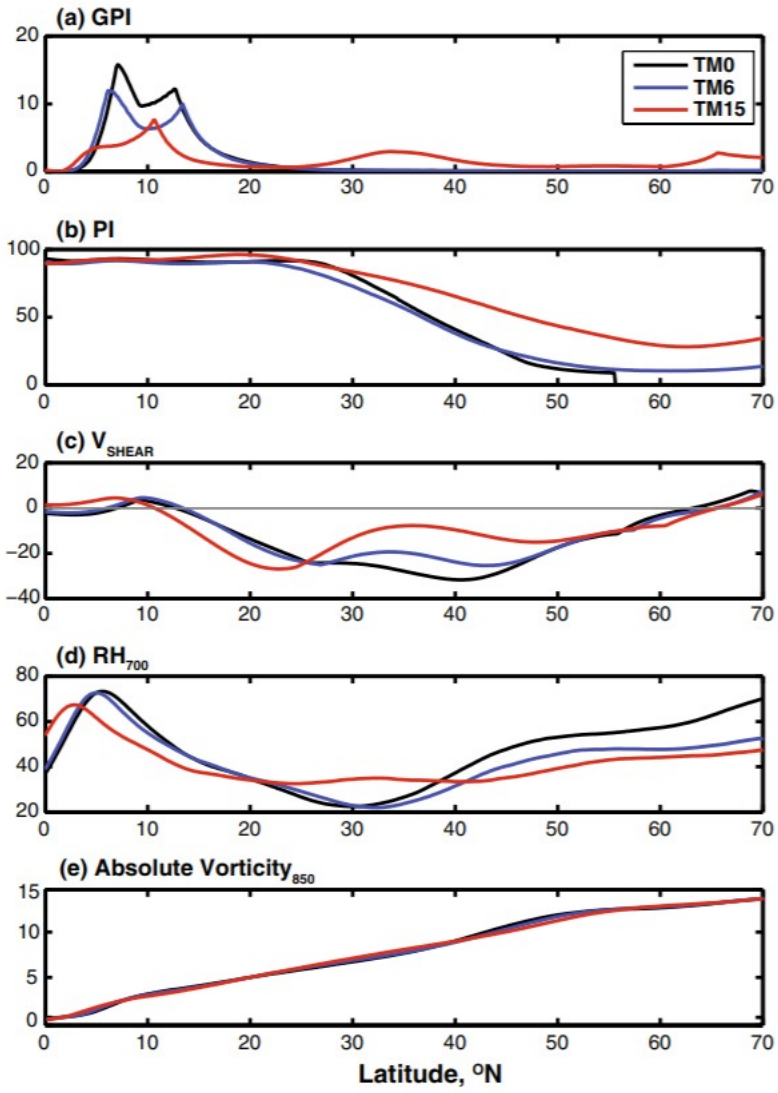

Fig. 10 The Genesis Potential Index (*GPI*) and its main components as a function of latitude for simulations TM0 (black), TM6 (blue), and TM15 (red). **a** GPI; **b** potential intensity, *PI* (m s^{-1}); **c** vertical shear defined as difference in wind speed between 850 and 200 mb, *V* (m s^{-1}); **d** relative humidity at 700 hPa, *H*; **e** absolute vorticity at 850 hPa, η (10^{-5} s^{-1}). Following Emanuel and Nolan (2004) we define *GPI* as $GPI = \left|10^5\eta\right|^{3/2}(H/50)^3(PI/70)^3(1+0.1V)^{-2}$

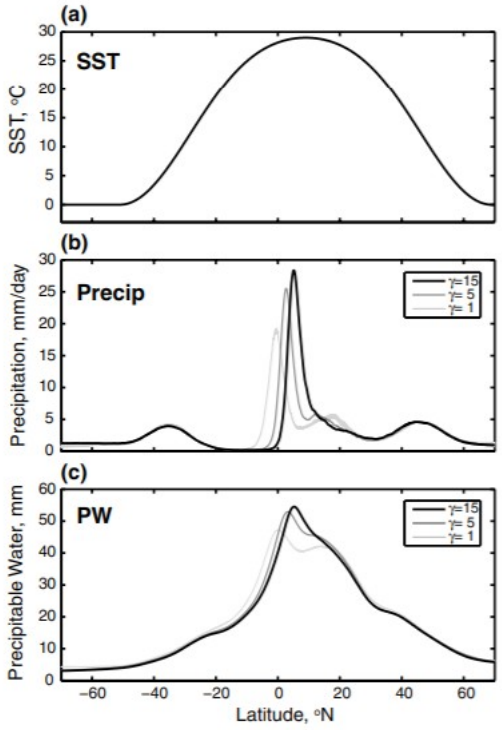

Fig. 11 Meridional distribution of **a** prescribed sea surface temperature (°C), and the simulated zonal means of **b** precipitation (mm/day) and (c) precipitable water (mm) for simulations using different RAVE numbers $\gamma = 1$ (light gray), $\gamma = 5$ (gray) and $\gamma = 15$ (black). Note that the ITCZ moves to a more northerly position, several degrees of latitude away from the equator, for higher RAVE numbers

In contrast, changes in TM15 are much more dramatic. The ITCZ weakens even more and moves closer to the equator, significantly reducing tropical cyclogenesis on the northern flank of the ITCZ (Figs. 2c, 6c), consistent with the strong drop in GPI between 5° and 20°N (Fig. 10a). However, a new region of cyclogenesis opens up within and around the band 30°–40°N, associated with a new maximum in GPI (Figs. 6c, 10a). This second GPI maximum largely accounts for changes in TC activity.

The GPI increase in mid-latitudes is related to three key factors—an increase in the potential intensity (PI) of TCs, an increase in mid-tropospheric relative humidity, and a decrease in vertical shear (Fig. 10b–d). TC potential intensity increases because of significantly higher extra-tropical SSTs; indeed, the increase in PI could be seen as resulting from an increase in relative SST[1] (Vecchi and Soden 2007; Ramsay and Sobel 2011). Another interpretation for PI increase can be in terms of the changing air–sea enthalpy disequilibrium (Emanuel and Sobel 2013). Relative humidity rises at least in part because of weaker subsidence due to a weaker Hadley circulation (note the anomalous ascent near 30°N in Fig. 3c). Lastly, vertical shear is modified by changes in the structure of atmospheric zonal flow—the weakening and splitting of the northern upper tropospheric jet creates a valley of weakened wind shear in between the subtropical and polar jets (Figs. 4c, 10c). A reduction of vertical

shear is already noticeable in TM6, but only in TM15 does it become large enough to cause the second maximum in GPI. These three factors together act to enhance the GPI in mid-latitudes, whereas changes in absolute vorticity between the simulations are fairly minor.

The jet split evident in Fig. 4 warrants some discussion. Note that these are summer-hemisphere jets that are distinct from winter-hemisphere subtropical jets governed by angular momentum-conserving dynamics. The jet between 20–30°N is in the summer Hadley cell and the jet between 40–50°N is in the Ferrel cell. Both jets are understood as eddy dominated, though the lower-latitude jet would still exist in axisymmetric models. We speculate that the jet split is related to two opposing tendencies:

1. The poleward shift and weakening of the mid-latitude jet associated with the expansion of the tropics and the reduction of equator-to-pole SST gradient. The detailed dynamics responsible for the poleward shift of jets, especially eddy-dominated jets in the summer hemisphere, has been an active area of research (Lehmann et al. 2014; Yin 2005) and we do not study the underlying mechanism here. However, the weakening of the eddy-driven mid-latitude jet may be related to a weakening of extratropical eddy activity; that eddy activity has been shown to scale with the mean available potential energy (O'Gorman 2010), which in turn decreases as the meridional temperature gradient weakens and as the tropospheric static stability increases.

2. Tendency of poleward propagating Rossby waves to transport eastward momentum toward the equator, which shifts the subtropical jet equatorward. This effect increases in warmer climates, ultimately leading to superrotation (e.g. Arnold et al. 2012; Caballero and Huber 2010).

The emergence of the second region of cyclogenesis has major consequences for the overall distribution of tropical cyclones. While the number of weak TCs (up to category 1) is still slightly smaller in TM15 than in TM0, the number of stronger cyclones (categories 2 through 5) increases several-fold (Figs. 7c, 9). As a result, the overall frequency of tropical cyclones increases, albeit slightly compared to TM0. Many of these strong TCs actually develop or reach their maximum strength relatively far north, between 30 and 40°N, in the region of reduced vertical shear (Figs. 6c, 7c).

At the same time, the number of warm-core extra-tropical cyclones increases greatly, by a factor of 7 or 8 (Table 1), suggesting the growing role of moist convection in warmer climates. Moreover, the properties of the two types of storms, tropical and extra-tropical, converge, as suggested by the overlapping of the two distributions in the pressure–velocity space and the storms' latitudes of origin (Fig. 7c). The convergence of the two groups is also evident from the cluster analysis (Figs. 14, 15, "Appendix 2"). Although the end members of the two distributions still remain very distinct, this convergence implies the appearance of a large number of "hybrid" warm-core storms having properties of both tropical and extra-tropical cyclones.

Consequently, establishing a clear boundary between the two groups, even by means of a formal cluster analysis, becomes problematic.

5 Discussion

We have conducted a suite of idealized simulations with a cloud-system resolving model to study the effect of reduced meridional SST gradient on tropical cyclogenesis on a global scale. To the best of our knowledge, this is the first attempt to use cloud or cloud-system resolving models to explore this problem. To improve the simulation of TCs and achieve a more realistic tropical mean state we used the RAVE rescaling (Kuang et al. 2005; Boos et al. 2016), which provides a useful alternative to convective parameterization.

We find that changes in TC activity induced by the reduction of the SST gradient are not monotonic, and may depend on an interplay between changes in the position of the ITCZ and changes in the extra-tropical atmospheric mean state. In particular, the imposed SST changes lead to an equatorward shift of the ITCZ in warmer climates (a detrimental effect for tropical cyclogenesis), whereas the low-level extra-tropical atmosphere becomes warmer and more humid, relative to the mean tropical atmosphere, while experiencing a reduction in vertical wind shear (favorable effects for cyclogenesis). As a result, for moderate reductions in the SST gradient, the changes in TC activity are relatively small, showing less frequent TCs. However, further reduction of the SST gradient towards values typical of past warm, equable climates has dramatic consequences for cyclogenesis. Specifically, the total number of warm-core cyclones (both TCs and ETCs), increases by more than a factor of two in our warmest simulation as compared to the modern (Table 1). The number of stronger TCs of categories 2 through 5 increases as well. These results are generally consistent with the findings of Fedorov et al. (2010) who simulated the early Pliocene climate by prescribing a strong reduction in the meridional SST gradient (Brierley et al. 2009), but highlight the possible emergence of a large population of hybrid storms in the most equable climates.

How realistic is the equatorward shift of the ITCZ simulated in our model's warmer climates? Merlis et al. (2013) studied the effect of climate change on tropical cyclogenesis on an aqua-planet using a slab-ocean atmospheric GCM with 50 km horizontal resolution and a fixed q-flux. In such a configuration the ITCZ moves northward when the radiative forcing (the solar constant or CO_2 concentration) is increased, leading to a monotonic increase in TC activity. This contrasts with our approach in which we use a prescribed SST forcing wherein the implied q-flux will vary across the simulations. Nevertheless, one generally expects the ITCZ to move toward the hemisphere having the largest SST increase (e.g. Chiang and Friedman 2012), consistent with the southward shift of the ITCZ in our TM15 integration. Recent theories that quantitatively predict ITCZ shifts are based on atmospheric energy fluxes rather than SSTs and so are typically applied in models with interactive SSTs (e.g. Kang et al. 2008); nevertheless these

theories successfully predict ITCZ latitude in models with prescribed SST (e.g. Shekhar and Boos 2016) and produce results consistent with the idea that the ITCZ will shift toward the hemisphere with the most SST warming.

The results of Ballinger et al. (2015), who used prescribed SSTs within a ~ 50 km atmospheric GCM with parameterized convection, are also consistent with the aforementioned idea—when they flattened the SST field in the northern low latitudes, thus reducing SST primarily in the northern hemisphere, the ITCZ moved equatorward. A further comparison with their results suggests that our experiments TM0 and TM6 show a generally similar behavior as their experiments (in terms of the preferable genesis latitude for example); our TM15 integration, however, has a much stronger change in the meridional SST gradient than any used by Ballinger et al. (2015). Note however that their study considers only those TCs that are equatorward of 25°N at their first detection, which can introduce a significant bias to their results.

In general, numerous influences on the ITCZ position have not been accounted for by Merlis et al. (2013), Ballinger et al. (2015), or our study. For example, the strength of the Atlantic meridional overturning circulation (AMOC), a major contributor to northward heat transport, is believed to be of global importance. The weakening of the AMOC cools the northern hemisphere relative to the southern hemisphere, forcing a southward shift of the ITCZ (e.g. Marshall et al. 2014; Schneider et al. 2014). Anomalous ocean currents induced by changes in atmospheric wind stress might also influence ITCZ position (e.g. Green and Marshall 2017); for a further discussion also see Boos and Korty (2016).

In the Pacific ocean the strong equatorial cold tongue is a major factor that keeps the ITCZ north of the equator (Xie and Philander 1994). A recent study suggested that on geological timescales the meridional (equator-to-pole) and zonal (east-to-west, along the equator) SST gradients are tightly linked in the Pacific (Fedorov et al. 2015). Consequently, in the coupled ocean–atmosphere system a reduction in the meridional SST gradient would induce a reduction in the equatorial zonal gradient and hence a weakening of the cold tongue. Many studies argued that during the warm Pliocene epoch some 3–5 million years ago, the cold tongue was indeed weaker (for a recent discussion see Fedorov et al. 2013, 2015; Manucharyan and Fedorov 2014; Ravelo et al. 2014), implying a more southerly position of the ITCZ (Burls and Fedorov 2014).

While our simulations are idealized, several aspects of the results may have implications for future changes in TC activity. For example, we find that the transition to warmer climates opens up a new zone of cyclogenesis in the extra-tropics, driven by a significant reduction in wind shear and an increase in maximum potential intensity and relative humidity. The latter factors imply a stronger role for moist convection in extra-tropical storms, which manifests in our simulations as the merging of the distributions of tropical

and warm-core extra-tropical cyclones and the emergence of a large number of hybrid cyclones sharing the properties of both. Such hybridization is relatively rare in the modern climate, with Hurricane Sandy being perhaps the most famous example (Blake et al. 2013). A shift of tropical cyclogenesis towards mid-latitudes in very warm climates has been also noted by Korty et al. (2017) who used a statistical downscaling approach with greenhouse-warming GCM simulations. A modest poleward migration of the location of tropical cyclone maximum intensity, plausibly linked to the ongoing tropical expansion due to anthropogenic global warming, has been also observed (Kossin et al. 2014).

There are a number of limitations to our study. For example, we use prescribed SST, which does not allow TCs to influence the state of the upper ocean. We actually began our simulations using interactive SST, but the increased computational demand associated with achieving a steady SST distribution prevented completion of these simulations. Consequently, we chose the simplest model set-up to address the two main goals of the study —to test the RAVE approach and to study gross changes in TC activity in warmer climates within a cloud-system resolving model. In the future, we will add a slab-ocean to the model. We expect that interactions between cloud-radiative processes, SST, and ITCZ location may increase the complexity of the response (Kang et al. 2008). Another important effect of ocean coupling on TC intensity is the wind-induced diapycnal mixing, which would require representation of entrainment of thermocline water into the ocean mixed layer (i.e. going beyond a simple slab-ocean model), which may reduce the intensity of some of the strongest cyclones, but should not affect the results on the whole.

Furthermore, to isolate the effect of the meridional SST gradient we keep the maximum SST fixed, even though it can change, albeit not as fast as extra-tropical SSTs (Ravelo et al. 2014; Fedorov et al. 2015; Huber and Caballero 2011). Also, we do not consider zonal differences or differences between ocean basins. To some extent, going from simulation TM0 to TM6 could be considered as switching from the Northeast Pacific, where SSTs are colder and where tropical and extra-tropical cyclones are well separated by genesis latitude, to the Northwest Pacific or North Atlantic where warmer extra-tropical SSTs typically allow tropical cyclones to propagate much farther north (as in Fig. 6b).

For computations we use a relatively coarse horizontal resolution (15 km) in combination with the RAVE rescaling ($\gamma = 15$). Using a resolution of 1–2 km in a cloud-resolving model would eliminate the necessity to use RAVE (Boos et al. 2016), but such simulations on a global scale are currently beyond our computational capabilities.

Despite these limitations, several major results of this study appear to be robust, in that they consist of high amplitude simulated changes with straightforward physical explanations. For sufficiently large reductions in

meridional SST gradient these include the increase in the number of strong cyclones, the establishment of a new TC genesis region in mid-latitudes, and the hybridization of tropical and extra-tropical storms. These effects should become even more pronounced if the ITCZ were to shift northward in conjunction with the reduction in SST gradient. Future studies will need to revisit this issue and also include the effects of interactive SST.

Footnotes

1.

The dependence of PI on relative SST (local SST minus a tropical mean SST) requires horizontal temperature gradients in the free-troposphere to be weak. Although the mid-latitude region in which PI increases lies outside the tropical domain in which weak temperature gradient theories are strictly valid, we still expect upper-tropospheric temperature gradients to be weaker than low-level gradients in equivalent potential temperature, so that relative SST will behave at least qualitatively like PI.

Acknowledgements

We thank two anonymous reviewers for their constructive comments on the paper. Financial support was provided by grants to AVF from the David and Lucile Packard Foundation, NSF (AGS-0163807), and NOAA (NA14OAR4310277). WRB was supported by Office of Naval Research award N000141512531. JS was supported by the Russian Foundation for Basic Research (grant #17-05-00509) and the Russian Science Foundation (grant #14-50-00095). Support from the Yale University Faculty of Arts and Sciences High Performance Computing facility is acknowledged.

Appendix 1: RAVE rescaling

To improve the simulation of tropical cyclogenesis, and also to achieve a mean tropical state more closely resembling observations, we use the Reduced Acceleration in the Vertical (RAVE) rescaling, which reduces the vertical velocities and increases the horizontal length scales of convective motions, in effect making them closer in size to those of the unaltered large-scale, nearly hydrostatic flow (e.g. Kuang et al. 2005; Pauluis and Garner 2006; Garner et al. 2007; Boos et al. 2016). RAVE is also referred to as the hypohydrostatic rescaling because it increases the inertia of vertical motion, and is implemented by multiplying the acceleration term in the vertical momentum equation by a factor $\gamma > 1$:

$$\gamma^2 \frac{Dw}{Dt} = -\frac{1}{\rho}\frac{\partial p}{\partial z} - g + F_z$$

Here, $\frac{Dw}{Dt}$ is the material derivative of vertical velocity, $-\frac{1}{\rho}\frac{\partial p}{\partial z}$ the acceleration due to the vertical pressure gradient, g the acceleration due to gravity, F_z the acceleration due to vertical diffusion, and γ is the RAVE factor. Choosing $\gamma = 1$ corresponds to the standard vertical momentum equation (no rescaling), while $\gamma = 0$ corresponds to the hydrostatic approximation.

The RAVE rescaling is mathematically equivalent to the Diabatic Acceleration and Rescaling (DARE), in which the planetary rotation rate and diabatic processes, such as radiative fluxes and surface enthalpy fluxes, are increased by the factor γ, while the planetary radius is decreased by γ. The DARE approach shrinks the time and space scales of the large-scale dynamics (e.g. the Rossby radius of deformation), bringing them closer to the scales of convective motions. Another related approach is known as the Deep Earth rescaling, in which the gravitational acceleration is decreased and the vertical coordinate is increased in scale by γ (Pauluis and Garner 2006). The same modification of the equations of motion was also used years earlier in numerical weather prediction in so-called quasi-nonhydrostatic models (Browning and Kreiss 1986; MacDonald et al. 2000). Although all of these treatments are mathematically identical, RAVE has the simplest physical interpretation and can be easily implemented in numerical models.

Kuang et al. (2005) conducted RAVE simulations of the atmospheric circulation on an equatorial β-plane with an ocean mixed-layer lower boundary, with emphasis on convectively coupled equatorial waves. Garner et al. (2007) conducted global aqua-planet simulations with large RAVE factors ($\gamma \geq 100$) and found that the extra-tropical circulation was largely unaltered by such extreme rescaling; they noted that use of RAVE with $\gamma \approx 3$ and horizontal resolutions on the order of 10 km may provide a promising alternative to convective parameterization. Ma et al. (2014) produced a remarkably accurate climatology of South Asian monsoon precipitation using RAVE in a global model (on a sphere) without convection parameterization, with a horizontal resolution of 40 km and $\gamma = 10$. Boos and Kuang (2010) used RAVE on an equatorial β-plane to examine the mechanisms involved in tropical intraseasonal variability in a model with horizontal resolution of about 30 km and $\gamma \approx 15$.

Realistic simulation of TCs typically requires model horizontal resolution on the order of 1 km in models without convective parameterization. Recently, Boos et al. (2016) studied convective self-aggregation and tropical cyclogenesis in doubly-periodic domains on an f-plane and showed that the RAVE approach could improve simulation of TCs in cloud-system resolving models with relatively coarse resolutions, on the order of 10 km. For the simulation of TCs, RAVE thus provides an attractive alternative to convective parameterization at resolutions in the so-called “gray zone”.

The conclusions of Boos et al. (2016) contradicted the earlier work of Pauluis and Garner (2006), who argued that RAVE worsened the dry bias in coarse resolution models; however, the authors of that earlier study did not consider that, since they were increasing their domain size as horizontal resolution was coarsened, convective self-aggregation and an associated domain-mean drying would occur at the coarser resolutions (e.g. Bretherton et al. 2005; Muller and Held 2012). Boos et al. (2016) showed that instead of increasing the humidity bias, RAVE actually reduces a dry bias caused by use of coarse resolution in simulations of radiative-convective equilibrium.

The present study builds on the results of Boos et al. (2016) but goes one step further and simulates both the atmospheric general circulation and tropical cyclogenesis on a global scale. Throughout the integrations described in the main text we used $\gamma = 15$, which, given the explicit grid spacing of 15 km, provides an "equivalent" rescaled horizontal resolution of 1 km (e.g. Pauluis and Garner 2006). Use of $\gamma = 15$ allowed our control integration (TM0) to produce a somewhat realistic representation of the modern zonal mean tropical climate state and tropical cyclones up to category 5. Here, we describe the differences between several simulations for our idealization of modern climate, using the same boundary conditions as in TM0, but increasing the value of γ from 1 to 5 and then to 15.

Without RAVE or with small RAVE factors the simulations exhibit a "double-ITCZ" problem—the ITCZ splits into two convergence zones, with the stronger one located on the southern flank of the SST maximum (Fig. 11b). This feature is not unlike the much discussed double-ITCZ problem in GCM simulations that produce two local maxima in precipitation in the eastern Pacific on opposite sides of the equator (e.g. Li and Xie 2014). For $\gamma = 1$, the stronger ITCZ sits 0.5° south of the equator, and is geographically well-separated from most tropical cyclogenesis events (Fig. 12a, b). A second, weaker convergence zone is located as far north as 20°N. As we increase γ to 5, the stronger ITCZ moves north of the equator while the secondary convergence zone weakens and shifts southward. Only for $\gamma = 15$ does the model simulate a single ITCZ, roughly at 5°N, not too far from the observed mean ITCZ position in the central Pacific in July (e.g. Schneider et al. 2014).

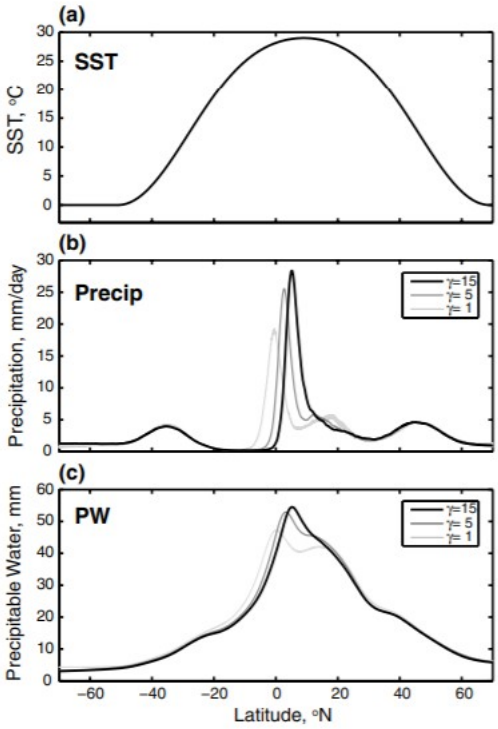

Fig. 11 Meridional distribution of **a** prescribed sea surface temperature (°C), and the simulated zonal means of **b** precipitation (mm/day) and (c) precipitable water (mm) for simulations using different RAVE numbers $\gamma = 1$ (light gray), $\gamma = 5$ (gray) and $\gamma = 15$ (black). Note that the ITCZ moves to a more northerly position, several degrees of latitude away from the equator, for higher RAVE numbers

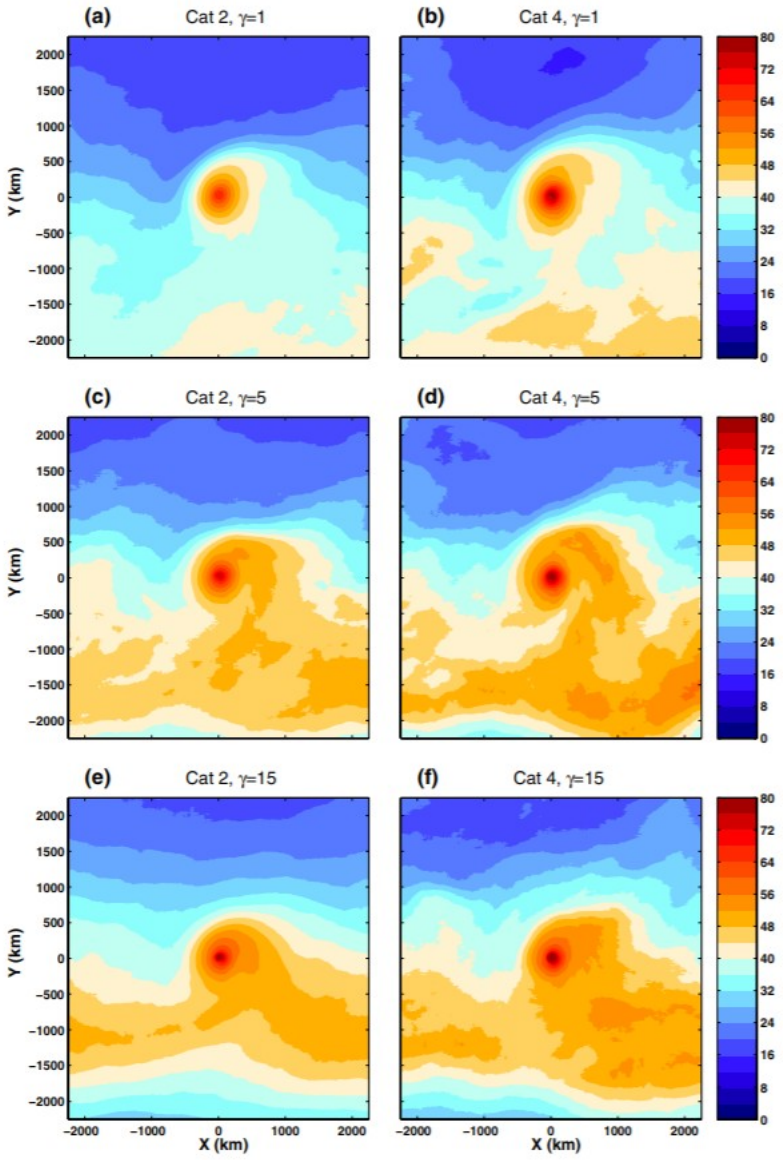

Fig. 12 Composites of (left) category 2 and (right) category 4 tropical cyclones, shed from the ITCZ and evident in the precipitable water field, for simulations using different RAVE numbers: $\gamma = 1$ (top), $\gamma = 5$ (middle), and $\gamma = 15$ (bottom). Note the environmental moistening over the cyclogenesis region (discussed by Boos et al. 2016) and a better representation of the hurricane eye for higher RAVE numbers

Why does using RAVE shift the ITCZ with respect to the SST maximum? This is a difficult question as it requires understanding the mechanisms that set the latitude of the ITCZ, given the SST distribution, and those mechanisms are not well understood (e.g. Back and Bretherton 2009; Schneider et al. 2014; Faulk et al. 2017). Boos et al. (2016) argued that RAVE increases the free-tropospheric humidity of the environment surrounding aggregated convection, and there is indeed an increase in precipitable water near and just north of the ITCZ, which is a type of aggregated convection, as γ is increased (Fig. 11c). Perhaps this increase in precipitable water allows convection near the SST maximum to be less inhibited by the entrainment of dry air, so that the ITCZ latitude is controlled more by thermodynamics (e.g. the latitude of maximum CAPE) than by boundary layer dynamics (e.g. Pauluis 2004). Other studies have shown that ITCZ latitude simulated in a GCM can be greatly influenced by the amount of entrainment required to

occur in parameterized deep convection (Kang et al. 2008); although that sensitivity was demonstrated to be mediated by cloud radiative effects in a model with interactive SST, our results show that ITCZ latitude can be greatly influenced by the details of moist convection even when SST is prescribed.

Unsurprisingly, increasing γ to 15 also affects tropical cyclogenesis. In particular, as γ is increased from 1 to 15, the number of tropical cyclones increases by roughly a factor of two, with the frequency of strong cyclones also increasing (Fig. 13). This increase in TC activity for sufficiently high RAVE numbers might occur because of three main factors. The first is the ITCZ shift to its northerly position where it can play a more active role in cyclogenesis (e.g. Merlis et al. 2013; Figs. 11, 12). The second is the general moistening of the environment around tropical cyclones (Figs. 12, 11), especially in the region of active cyclogenesis, consistent with the argument of Boos et al. (2016). The third factor is a better representation of the core of the cyclones, specifically the hurricane eye and eyewall, and more coherent convective bands (Fig. 12).

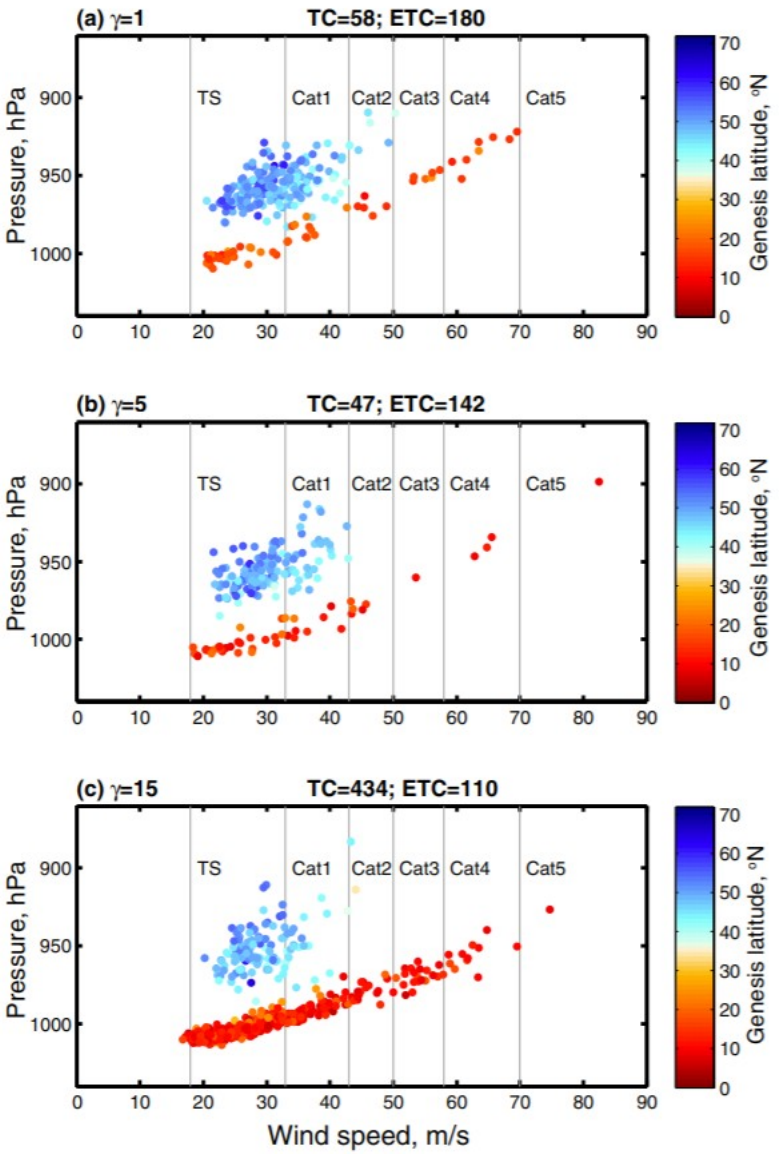

Fig. 13 Scatterplots of maximum surface wind speed (m/s) versus minimum central surface pressure (hPa) for warm-core cyclones in perpetual July simulations using different RAVE numbers: **a** $\gamma = 1$, **b** $\gamma = 5$, and **c** $\gamma = 15$. Each point is colored according to the cyclone's genesis latitude; the Saffir–Simpson categories are also shown. Note the significant increase in the number of tropical cyclones, including strong storms, for $\gamma = 15$. The numbers at the top of each panel refer to the total number of tropical (TC) and extra-tropical (ETC) cyclones in the simulations. The bottom panel is identical to Fig. 7a. Each simulation lasts 20 boreal summers

Appendix 2: Tracking algorithm and cyclone clustering

To track warm-core cyclones we follow the algorithm of Scoccimarro et al. (2011), closely related to that of Walsh et al. (2007). We first identify all cyclonic vortices above a given vorticity threshold at 850 hPa. Then we find the sea level pressure (SLP) minimum within a 350 km radius of the vorticity maximum. This location is now a candidate for a cyclone, which we subject to several key tests:

Test 1

Vorticity maximum at 850 hPa is above the threshold η_{min}.

Here we use $\eta_{min} = 10^{-5} s^{-1}$.

Test 2

SLP minimum is 2 hPa lower than SLP averaged within a 350 km radius from the vorticity maximum.

Test 3

Surface wind speed maximum is greater than 15.5 ms^{-1} (within a 350 km radius).

Test 4

Average wind speed over inner 50 km is greater at 850 hPa than at 300 hPa

Test 5

The cyclone has a warm core. That is, the temperature anomaly, in the location of the maximum vorticity, estimated as $T' = T'_{300\ hPa} + T'_{500\ hPa} + T'_{700\ hPa}$, is positive and $T' > 1$ °C

Test 6

The core temperature is warmer than temperature averaged within a 350 km radius from the vorticity maximum

Finally, to obtain the cyclone tracks we connect locations of each vortex at different time steps separated by 6 h, as long as the vortex has persisted for a minimum of 24 h and its center has not moved more than 350 km in 6 h. The cyclone tracks shown in Fig. 6 are obtained through this procedure. For the distributions shown in Figs. 7 and 13 we pick up the strongest values of surface wind speed along the tracks and the corresponding values of SLP.

To further investigate how the distributions of tropical and warm-core extra-tropical cyclones change with SST gradient we use a formal clustering technique to separate storms of different origin according to their physical characteristics. In particular, separation based on the 200 and 800 hPa geopotential heights works especially well for the modern climate since ETCs are typically too shallow to produce large fractional changes in upper tropospheric heights (Fig. 14). The computation of the clusters follows Studholme et al. (2015) and uses the k-means algorithm (e.g. Lloyd 1982, here $k = 2$). It involves grouping cyclones into k clusters by minimizing the sum of squares of Euclidean distances to each cluster's centroid within the 200 and 800 hPa geopotential height phase space for all identified warm-core cyclones.

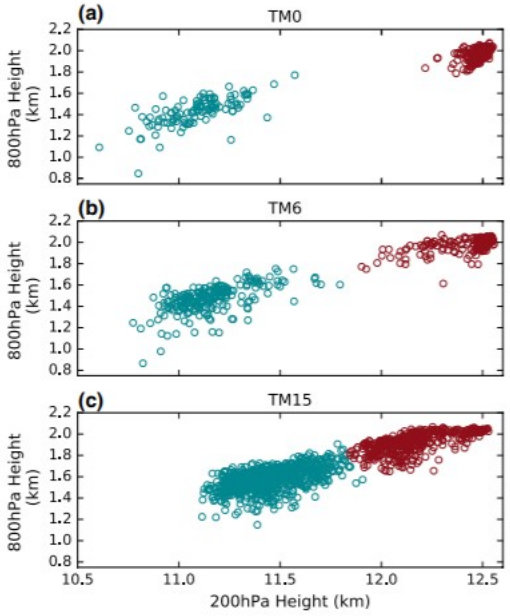

Fig. 14 Scatterplots of simulated warm-core cyclones in terms of 200 and 800 hPa geopotential heights in different simulations: **a** TM0, **b** TM6, and **c** TM15. Two distinct clusters of storms are identified—Tropical (red) and Extra-tropical (blue-green). These two clusters merge in the TM15 simulation. Even though the clustering analysis draws a boundary between the two clusters in the last simulation, the properties of storms change gradually across this boundary

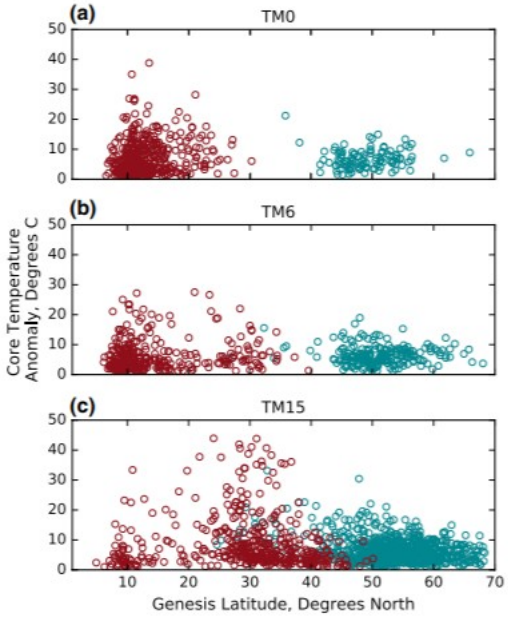

Fig. 15 The same two clusters as in Fig. 14, Tropical (red) and Extra-tropical (blue–green), but shown in terms of core temperature anomaly and genesis latitude for **a** TM0, **b** TM6, and **c** TM15. The plot further illustrates that the two clusters in TM15 overlap as tropical cyclones can develop much farther north in this simulation

Reducing the meridional SST gradient acts to reduce the “distance” between the clusters in the TM6 simulation and eventually to merge the two clusters in TM15 (Fig. 14c). In terms of core temperature anomalies, extra-tropical cyclones are typically a little colder than tropical cyclones, as they originate farther north (Fig. 15). Nevertheless, where the two distributions overlap in mid-latitudes in TM15, their properties become quite similar.

References

Arnold NP, Randall DA (2015) Global-scale convective aggregation: implications for the Madden–Julian oscillation. J Adv Model Earth Syst 7:1499–1518. https://doi.org/10.1002/2015MS000498.

Arnold NP, Tziperman E, Farrell B (2012) Abrupt transition to strong superrotation driven by equatorial wave resonance in an idealized GCM. J Atmos Sci 69:626–640. https://doi.org/10.1175/JAS-D-11-0136.1

Back LE, Bretherton CS (2009) A simple model of climatological rainfall and vertical motion patterns over the tropical oceans. J Clim 22:6477–6497. https://doi.org/10.1175/2009JCLI2393.1

Ballinger AP, Merlis TM, Held IM, Zhao M (2015) The sensitivity of tropical cyclone activity to off-equatorial thermal forcing in aquaplanet simulations. J Atmos Sci. https://doi.org/10.1175/JAS-D-14-0284.1

Bender MA, Knutson TR, Tuleya RE, Sirutis JJ, Vecchi GA, Garner ST, Held IM (2010) Modeled impact of anthropogenic warming on the frequency of intense Atlantic Hurricanes. Science (80-.) 327:454–458

Bengtsson L, Hodges KI, Esch M, Keenlyside N, Kornblueh L, Luo J-J, Yamagata T (2007) How may tropical cyclones change in a warmer climate? Tellus A Dyn Meteorol Oceanogr 59:539–561. https://doi.org/10.1111/j.1600-0870.2007.00251.x

Bister M, Emanuel KA (1998) Dissipative Heating and Hurricane Intensity. Meteorol Atmos Phys 65:233–240

Blake ES, Kimberlain TB, Berg RJ, Cangialosi GP, Beven JL II (2013) Tropical cyclone report: Hurricane Sandy. National Hurricane Center Tech. Rep. AL182012, 22–29 October 2012. https://data.globalchange.gov/reference/13960922-e064-4be9-97cc-83572b69b666

Boos WR, Korty RL (2016) Regional energy budget control of the intertropical convergence zone and application to mid-Holocene rainfall. Nat Geosci 9:892–897. https://doi.org/10.1038/ngeo2833

Boos WR, Kuang Z (2010) Mechanisms of poleward propagating, intraseasonal convective anomalies in cloud system–resolving models. J Atmos Sci 67:3673–3691. https://doi.org/10.1175/2010JAS3515.1

Boos W, Muir L, Fedorov AV (2016) Convective self-aggregation and tropical cyclogenesis under the hypohydrostatic rescaling. J Atmos Sci 73:525–544

Bretherton CS, Khairoutdinov MF (2015) Convective self-aggregation feedbacks in near-global cloud-resolving simulations of an aquaplanet. J Adv Model Earth Syst 7:1765–1787. https://doi.org/10.1002/2015MS000499

Bretherton CS, Blossey PN, Khairoutdinov M (2005) An energy-balance analysis of deep convective self-aggregation above uniform SST. J Atmos Sci 62:4273–4292

Brierley C, Fedorov AV, Liu Z, Herbert T, Lawrence K, LaRiviere J (2009) Greatly expanded tropical warm pool and weaker Hadley circulation in the early Pliocene. Science 323:1714–1117

Browning GL, Kreiss H-O (1986) Scaling and computation of smooth atmospheric motions. Tellus A 38A:295–313. https://doi.org/10.1111/j.1600-0870.1986.tb00417.x

Burls NJ, Fedorov AV (2014) What controls the mean east–west sea surface temperature gradient in the equatorial Pacific: the role of cloud albedo. J Clim 27:2757–2778. https://doi.org/10.1175/JCLI-D-13-00255.1

Burls N, Fedorov AV (2017) Wetter subtropics in a warmer world: contrasting past and future hydrological cycles. PNAS. https://doi.org/10.1007/s00382-016-3435-6

Burls N, Vincent E, Muir L, Fedorov AV (2016) Extra-tropical origin of equatorial Pacific cold bias in climate models with links to cloud albedo. Clim Dyn. https://doi.org/10.1073/pnas.1703421114

Caballero R, Huber M (2010) Spontaneous transition to superrotation in warm climates simulated by CAM3. Geophys Res Lett. https://doi.org/10.1029/2010GL043468

Camargo SJ (2013) Global and regional aspects of tropical cyclone activity in the CMIP5 models. J Clim 26:9880–9902. https://doi.org/10.1175/JCLI-D-12-00549.1

Camargo SJ, Ting M, Kushnir Y (2013) Influence of local and remote SST on North Atlantic tropical cyclone potential intensity. Clim Dyn 40:1515–1529. https://doi.org/10.1007/s00382-012-1536-4

Camargo SJ et al (2014a) Testing the performance of tropical cyclone genesis indices in future climates using the HiRAM model. J Clim 27:9171–9196. https://doi.org/10.1175/JCLI-D-13-00505.1

Camargo SJ, Tippett MK, Sobel AH, Vecchi GA, Zhao M (2014b) Testing the performance of tropical cyclone genesis indices in future climates using the HiRAM model. J Clim 27:9171–9196. https://doi.org/10.1175/JCLI-D-13-00505.1

Carmichael MJ, Lunt DJ, Huber M, Heinemann M, Kiehl J, LeGrande A, Loptson CA, Roberts CD, Sagoo N, Shields C, Valdes PJ, Winguth A, Winguth C, Pancost RD (2016) A model-model and data-model comparison for the early Eocene hydrological cycle. Clim Past 12:455–481. https://doi.org/10.5194/cp-12-455-2016

Chiang JCH, Friedman AR (2012) Extratropical cooling, interhemispheric thermal gradients, and tropical climate change. Annu Rev Earth Planet Sci 40:383–412. https://doi.org/10.1146/annurev-earth-042711-105545

Emanuel KA (1988) The maximum intensity of hurricanes. J Atmos Sci 45:1143–1155

Emanuel KA (1995) Sensitivity of tropical cyclones to surface exchange coefficients and a revised steady-state model incorporating eye dynamics. J Atmos Sci 52:3969–3976

Emanuel KA (2005) Increasing destructiveness of tropical cyclones over the past 30 years. Nature 436:686–688. https://doi.org/10.1038/nature03906

Emanuel KA (2013a) Downscaling CMIP5 climate models shows increased tropical cyclone activity over the 21st century. Proc Natl Acad Sci USA 110:12219–12224. https://doi.org/10.1073/pnas.1301293110

Emanuel KA (2013b) Response of downscaled tropical cyclones to climate forcing: results and interpretation. In: U.S. CLIVAR hurricane workshop. 2013, Geophysical Fluid Dynamics Laboratory, Princeton, NJ, June 5–7

Emanuel KA, Nolan D (2004) Tropical cyclone activity and the global climate system. In: 26th Conf. on hurricanes and tropical meteorology. American Meteor Society, 10A.2, Miami, FL

Emanuel KA, Sobel A (2013) Response of tropical sea surface temperature, precipitation, and tropical cyclone-related variables to changes in global and local forcing. J Adv Model Earth Syst 5:447–458. https://doi.org/10.1002/jame.20032

Emanuel KA, Callaghan J, Otto PK (2008) A hypothesis for the redevelopment of warm-core cyclones over Northern Australia*. Mon Weather Rev 136:3863–3872. https://doi.org/10.1175/2008MWR2409.1

Emanuel K, Wing AA, Vincent EM (2014) Radiative-convective instability. J Adv Model Earth Syst 6:75–90. https://doi.org/10.1002/2013MS000270

Faulk S, Mitchell J, Bordoni S (2017) Effects of rotation rate and seasonal forcing on the ITCZ extent in planetary atmospheres. J Clim. https://doi.org/10.1175/JAS-D-16-0014.1

Fedorov AV, Brierley CM, Emanuel KA (2010) Tropical cyclones and permanent El Niño in the early Pliocene epoch. Nature 463:1066–1070. https://doi.org/10.1038/nature08831

Fedorov AV, Lawrence K, Liu Z, Brierley C, Dekens P, Ravelo AC (2013) Patterns and mechanisms of early Pliocene warmth. Nature 496:43–49

Fedorov AV, Burls N, Lawrence K, Peterson L (2015) Tightly linked ocean zonal and meridional temperature gradients over geological timescales. Nat Geosci 8:975–980

Fierro AO, Rogers RF, Marks FD, Nolan DS (2009) The impact of horizontal grid spacing on the microphysical and kinematic structures of strong tropical cyclones simulated with the WRF-ARW model. Mon Weather Rev 137:3717–3743

Garner ST et al (2007) Resolving convection in a global hypohydrostatic model. J Atmos Sci 64:2061–2075. https://doi.org/10.1175/JAS3929.1

Gentry MS, Lackmann GM (2010) Sensitivity of simulated tropical cyclone structure and intensity to horizontal resolution. Mon Weather Rev 138:688–704

Green B, Marshall J (2017) Coupling of trade winds with ocean circulation damps ITCZ shifts. J Clim 30:4395–4411

Gualdi S, Scoccimarro E, Navarra A (2008) Changes in tropical cyclone activity due to global warming: results from a high-resolution coupled general circulation model. J Clim 21:5204–5228. https://doi.org/10.1175/2008JCLI1921.1

Held IM, Zhao M (2011) The response of tropical cyclone statistics to an increase in CO_2 with fixed sea surface temperatures. J Clim 24:5353–5364. https://doi.org/10.1175/JCLI-D-11-00050.1

Huber M, Caballero R (2011) The early Eocene equable climate problem revisited. Clim Past 7:603

Huang A, Li H, Sriver RL, Fedorov AV, Brierley CM (2017) Regional variations in the ocean response to tropical cyclones: ocean mixing versus low cloud suppression. Geophys Res Lett 44(4):1947–1955

Kang SM, Held IM, Frierson DMW, Zhao M (2008) The response of the ITCZ to extratropical thermal forcing: idealized slab-ocean experiments with a GCM. J Clim 21:3521–3532. https://doi.org/10.1175/2007JCLI2146.1

Khairoutdinov MF, Randall DA (2003) Cloud resolving modeling of the ARM summer 1997 IOP: model formulation, results, uncertainties, and sensitivities. J Atmos Sci 60:607–625

Kiehl JT et al (1998) The national center for atmospheric research community climate model: CCM3*. J Clim 11:1131–1149

Kiehl JT, Shields CA, Khairoutdinov M (2012) Hurricanes during the Paleocene-Eocene thermal maximum. In: AGU fall meeting abstracts

Kim D et al (2012) The tropical subseasonal variability simulated in the NASA GISS general circulation model. J Clim 25:4641–4659. https://doi.org/10.1175/JCLI-D-11-00447.1

Knutson TR, Tuleya RE (2004) Impact of CO_2-induced warming on simulated hurricane intensity and precipitation: sensitivity to the choice of climate model and convective parameterization. J Clim 17:3477–3495. https://doi.org/10.1175/1520-0442(2004)017<3477:IOCWOS>2.0.CO;2.

Knutson TR et al (2007) Simulation of the recent multidecadal increase of Atlantic Hurricane activity using an 18-km-grid regional model. Bull Am Meteorol Soc 88:1549–1565. https://doi.org/10.1175/BAMS-88-10-1549

Knutson TR et al (2013) Dynamical downscaling projections of twenty-first-century Atlantic hurricane activity: CMIP3 and CMIP5 model-based scenarios. J Clim 26:6591–6617. https://doi.org/10.1175/JCLI-D-12-00539.1

Korty RL, Emanuel KA, Scott JR (2008) Tropical cyclone-induced upper-ocean mixing and climate: application to equable climates. J Clim 21:638–654. https://doi.org/10.1175/2007JCLI1659.1

Korty RL, Emanuel KA, Huber M, Zamora RA (2017) Tropical cyclones downscaled from simulations with very high carbon dioxide levels. J Clim 30:649–667. https://doi.org/10.1175/JCLI-D-16-0256.1

Kossin JP, Emanuel KA, Vecchi GA (2014) The poleward migration of the location of tropical cyclone maximum intensity. Nature 509:349–352, https://doi.org/10.1038/nature13278

Kuang Z, Blossey PN, Bretherton CS (2005) A new approach for 3D cloud-resolving simulations of large-scale atmospheric circulation. Geophys Res Lett 32:L02809. https://doi.org/10.1029/2004GL021024

Lehmann J, Coumou D, Frieler K, Eliseev AV, Levermann A (2014) Future changes in extratropical storm tracks and baroclinicity under climate change. Environ Res Lett 9:84002. https://doi.org/10.1088/1748-9326/9/8/084002

Li G, Xie S-P (2014) Tropical biases in CMIP5 multimodel ensemble: the excessive equatorial Pacific cold tongue and double ITCZ problems. J Clim 27:1765–1780. https://doi.org/10.1175/JCLI-D-13-00337.1

Lloyd SP (1982) Least squares quantization in PCM. IEEE Trans Inf Theory 28:129–137

Ma D, Boos W, Kuang Z (2014) Effects of orography and surface heat fluxes on the south Asian summer monsoon. J Clim 27:6647–6659. https://doi.org/10.1175/JCLI-D-14-00138.1

MacDonald AE, Lee JL, Sun S (2000) QNH: design and test of a quasi-nonhydrostatic model for mesoscale weather prediction. Mon Weather Rev 128:1016–1036. https://doi.org/10.1175/1520-0493(2000)128<1016:QDATOA>2.0.CO;2

Manucharyan G, Fedorov AV (2014) Robust ENSO across climates with different east-west equatorial SST gradients. J Clim 27:5836–5850

Marshall J, Donohoe A, Ferreira D, McGee D (2014) The ocean’s role in setting the mean position of the inter-tropical convergence zone. Clim Dyn 42:1967–1979. https://doi.org/10.1007/s00382-013-1767-z

Maue RN, Hart RE (2005) Warm-seclusion extratropical cyclone development: sensitivity to the nature of the incipient vortex. In: 21st conference on weather analysis and forecasting/17th conference on numerical weather prediction. Abstract P1.16

Merlis TM, Zhao M, Held IM (2013) The sensitivity of hurricane frequency to ITCZ changes and radiatively forced warming in aquaplanet simulations. Geophys Res Lett 40:4109–4114. https://doi.org/10.1002/grl.50680

Merlis TM, Zhou W, Held IM, Zhao M (2016) Surface temperature dependence of tropical cyclone-permitting simulations in a spherical model with uniform thermal forcing. Geophys Res Lett 43:2859–2865. https://doi.org/10.1002/2016GL067730

Miyamoto Y, Satoh M, Tomita H, Oouchi K, Yamada Y, Kodama C, Kinter III J (2014) Gradient wind balance in tropical cyclones in high-resolution global experiments. Mon Weather Rev 142:1908–1926. https://doi.org/10.1175/MWR-D-13-00115.1

Muller CJ, Held IM (2012) Detailed investigation of the self-aggregation of convection in cloud-resolving simulations. J Atmos Sci 69:2551–2565. https://doi.org/10.1175/JAS-D-11-0257.1

Murakami H, Arakawa O, Li T (2014) Influence of model biases on projected future changes in tropical cyclone frequency of occurrence*. J Clim 27:2159–2181. https://doi.org/10.1175/JCLI-D-13-00436.1

Neale RB, Hoskins BJ (2000) A standard test for AGCMs including their physical parametrizations I: the proposal. Atmos Sci Lett 1:101–107. https://doi.org/10.1006/asle.2000.0022

O'Gorman PA (2010) Understanding the varied response of the extratropical storm tracks to climate change. Proc Natl Acad Sci USA 107:19176–19180. https://doi.org/10.1073/pnas.1011547107

Pauluis O (2004) Boundary layer dynamics and cross-equatorial Hadley circulation. J Atmos Sci 61:1161–1173. https://doi.org/10.1175/1520-0469(2004)061<1161:BLDACH>2.0.CO;2

Pauluis O, Garner S (2006) Sensitivity of radiative–convective equilibrium simulations to horizontal resolution. J Atmos Sci 63:1910–1923. https://doi.org/10.1175/JAS3705.1

Ramsay HA, Sobel AH (2011) Effects of relative and absolute sea surface temperature on tropical cyclone potential intensity using a single-column model. J Clim 24:183–193. https://doi.org/10.1175/2010JCLI3690.1

Ravelo AC, Fedorov AV, Lawrence K, Ford H (2014) Comment on "A 12-million-year temperature history of the tropical Pacific Ocean". Science 346:1467–1468

Schneider T, Bischoff T, Haug GH (2014) Migrations and dynamics of the intertropical convergence zone. Nature 513:45–53

Scoccimarro E et al (2011) Effects of tropical cyclones on ocean heat transport in a high-resolution coupled general circulation model. J Clim 24:4368–4384

Shaevitz DA et al (2014) Characteristics of tropical cyclones in high-resolution models in the present climate. J Adv Model Earth Syst 6:1154–1172. https://doi.org/10.1002/2014MS000372

Shekhar R, Boos WR (2016) Improving energy-based estimates of monsoon location in the presence of proximal deserts. J Clim 29:4741–4761

Shi X, Bretherton CS (2014) Large-scale character of an atmosphere in rotating radiative-convective equilibrium. J Adv Model Earth Syst 6:616–629. https://doi.org/10.1002/2014MS000342

Studholme J, Hodges KI, Brierley CM (2015) Objective determination of the extratropical transition of tropical cyclones in the Northern Hemisphere. Tellus Ser A Dyn Meteorol Oceanogr. https://doi.org/10.3402/tellusa.v67.24474

Sugi M, Noda A, Sato N (2002) Influence of the global warming on tropical cyclone climatology: an experiment with the JMA global model. J Meteorol Soc Jpn 80:249–272

Sugi M, Noda A, Murakami H, Yoshimura J (2009) A reduction in global tropical cyclone frequency due to global warming. SOLA 5:164–167. https://doi.org/10.2151/sola.2009-042

Sun Y, Yi L, Zhong Z, Hu Y, Ha Y (2013) Dependence of model convergence on horizontal resolution and convective parameterization in simulations of a tropical cyclone at gray-zone resolutions. J Geophys Res Atmos 118:7715–7732. https://doi.org/10.1002/jgrd.50606

Tippett MK, Camargo SJ, Sobel AH (2011) A Poisson regression index for tropical cyclone genesis and the role of large-scale vorticity in genesis. J Clim 24:2335–2357. https://doi.org/10.1175/2010JCLI3811.1

Tory KJ, Chand SS, Dare RA, McBride JL (2013) An assessment of a model-, grid-, and basin-independent tropical cyclone detection scheme in selected CMIP3 global climate models. J Clim 26:5508–5522. https://doi.org/10.1175/JCLI-D-12-00511.1

Vecchi GA, Soden BJ (2007) Global warming and the weakening of the tropical circulation. J Clim 20:4316–4340. https://doi.org/10.1175/JCLI4258.1

Villarini G, Vecchi GA (2012) Twenty-first-century projections of North Atlantic tropical storms from CMIP5 models. Nat Clim Chang 2:604–607. https://doi.org/10.1038/nclimate1530

Walsh KJE, Fiorino M, Landsea CW, McInnes KL (2007) Objectively determined resolution-dependent threshold criteria for the detection of tropical cyclones in climate models and reanalyses. J Clim 20:2307–2314. https://doi.org/10.1175/JCLI4074.1

Walsh K, Lavender S, Scoccimarro E, Murakami H (2013) Resolution dependence of tropical cyclone formation in CMIP3 and finer resolution models. Clim Dyn 40:585–599. https://doi.org/10.1007/s00382-012-1298-z

Walsh KJE et al (2015) Hurricanes and climate: the U.S. CLIVAR working group on hurricanes. Bull Am Meteorol Soc 96:997–1017. https://doi.org/10.1175/BAMS-D-13-00242.1

Wing A, Emanuel KA (2014) Physical mechanisms controlling self-aggregation of convection in idealized numerical modeling simulations. J Adv Model Earth Syst. https://doi.org/10.1002/2013MS000269

Wu L et al (2014) Simulations of the present and late-twenty-first-century western north pacific tropical cyclone activity using a regional model. J Clim 27:3405–3424. https://doi.org/10.1175/JCLI-D-12-00830.1

Xie S-P, Philander SGH (1994) A coupled ocean-atmosphere model of relevance to the ITCZ in the eastern Pacific. Tellus A 46:340–350. https://doi.org/10.1034/j.1600-0870.1994.t01-1-00001.x

Yan Q, Wei T, Korty RL, Kossin JP, Zhang Z, Wang H (2016) Enhanced intensity of global tropical cyclones during the mid-Pliocene warm period. Proc Natl Acad Sci 113:12963–12967. https://doi.org/10.1073/pnas.1608950113

Yin JH (2005) A consistent poleward shift of the storm tracks in simulations of 21st century climate. Geophys Res Lett. https://doi.org/10.1029/2005GL023684

Yoshimura J, Sugi M (2005) Tropical cyclone climatology in a high-resolution AGCM—impacts of SST warming and CO_2 increase. Sola 1:133–136. https://doi.org/10.2151/sola.2005-035

Zhao M, Held IM (2010) An analysis of the effect of global warming on the intensity of Atlantic hurricanes using a GCM with statistical refinement. J Clim 23:6382–6393. https://doi.org/10.1175/2010JCLI3837.1

Zhao M, Held IM, Lin S-J (2012) Some counterintuitive dependencies of tropical cyclone frequency on parameters in a GCM. J Atmos Sci 69:2272–2283. https://doi.org/10.1175/JAS-D-11-0238.1